Copyright Warning & Restrictions

The copyright law of the United States (Title 17, United States Code) governs the making of photocopies or other reproductions of copyrighted material.

Under certain conditions specified in the law, libraries and archives are authorized to furnish a photocopy or other reproduction. One of these specified conditions is that the photocopy or reproduction is not to be "used for any purpose other than private study, scholarship, or research." If a, user makes a request for, or later uses, a photocopy or reproduction for purposes in excess of "fair use" that user may be liable for copyright infringement,

This institution reserves the right to refuse to accept a copying order if, in its judgment, fulfillment of the order would involve violation of copyright law.

Please Note: The author retains the copyright while the New Jersey Institute of Technology reserves the right to distribute this thesis or dissertation

Printing note: If you do not wish to print this page, then select "Pages from: first page # to: last page #" on the print dialog screen

NJIT New Jersey's Science & Technology University

The Van Houten library has removed some of the personal information and all signatures from the approval page and biographical sketches of theses and dissertations in order to protect the identity of NJIT graduates and faculty.

ABSTRACT

CHARACTERIZATION OF NEURAL ION REGULATION DYSFUNCTION DURING INSULT AND EVALUATION OF μ-OPIOID RECEPTOR ACTIVATION DURING SIMULATED ISCHEMIA IN THE PRE-BÖTZINGER COMPLEX

by
Kyle F. Dobiszewski

The health and vitality of brain tissue is dependent upon the cells' abilities to maintain ionic homeostasis across their plasma membranes. Even slight alterations in intracellular or extracellular can have a devastating effect on excitability and neural vitality. This thesis investigates several concepts related to ion flux. First, it investigates how ion flux affects characterization of brain tissue by dielectric spectroscopy and what can be done to overcome that effect. Second, it investigates how ion flux can be used to describe the state of health of the tissue. Finally, it investigates if pharmacological intervention can attenuate some of the deleterious ion flux seen in different pathologies.

The accumulation of ions in the extracellular fluid affects the use of dielectric spectroscopy to analyze the system. To attenuate this effect, a superfusion system was designed and built to provide fresh extracellular solution to the tissue. Furthermore, dielectric spectroscopy was utilized to analyze the change in conductivity of the extracellular solution as a result of various simulated pathologies. The change in conductivity was directly related to the severity of the insult. Finally, the ability of mu-opioid receptor activation to attenuate some of the damaging accumulation of extracellular potassium during simulated ischemia. The activation of this receptor proved to significantly modulate the accumulation of this potassium.

CHARACTERIZATION OF NEURAL ION REGULATION DYSFUNCTION DURING INSULT AND EVALUATION OF μ-OPIOID RECEPTOR ACTIVATION DURING SIMULATED ISCHEMIA IN THE PRE-BÖTZINGER COMPLEX

by
Kyle F. Dobiszewski

A Dissertation
Submitted to the Faculty of
New Jersey Institute of Technology
in Partial Fulfillment of the Requirements for the Degree of
Doctor of Philosophy in Materials Science and Engineering

Interdisciplinary Program in Materials Science and Engineering

August 2013

Copyright © 2013 by Kyle F. Dobiszewski

ALL RIGHTS RESERVED

.

APPROVAL PAGE

CHARACTERIZATION OF NEURAL ION REGULATION DYSFUNCTION DURING INSULT AND EVALUATION OF μ-OPIOID RECEPTOR ACTIVATION DURING SIMULATED ISCHEMIA IN THE PRE-BÖTZINGER COMPLEX

Kyle F. Dobiszewski

Dr. Camelia Prodan, Dissertation Co-Advisor — Date
Associate Professor of Physics, NJIT

Dr. Andrew Hill, Dissertation Co-Advisor — Date
Assistant Professor of Biological Sciences, NJIT

Dr. Gordon Thomas, Committee Member — Date
Professor of Physics, NJIT

Dr. Reginald Farrow, Committee Member — Date
Research Professor of Physics, NJIT

Dr. Bryan Pfister, Committee Member — Date
Associate Professor of Biomedical Engineering, NJIT

Dr. Alokik Kanwal, Committee Member — Date
Assistant Research Professor of Physics, NJIT

BIOGRAPHICAL SKETCH

Author: Kyle Francis Dobiszewski

Degree: Doctor of Philosophy

Date: August 2013

Undergraduate and Graduate Education:

- Doctor of Philosophy in Materials Science and Engineering,
  New Jersey Institute of Technology, Newark, NJ, 2013

- Bachelor of Science in Biomedical Engineering,
  New Jersey Institute of Technology, Newark, NJ, 2009

Major: Materials Science and Engineering

Presentations and Publications:

Dobiszewski KF, Deek MP, Ghaly A, Prodan C, Hill AA (2012) “Extracellular Fluid Conductivity Analysis by Dielectric Spectroscopy (DS) for In Vitro Determination of Cortical Tissue Vitality” Physiological Measurement 33(7) 1249-60

Dobiszewski KF, Shaker MR, Deek MP, Prodan C, Hill AA (2011) “Design and Implementation of a Novel Superfusion System for Ex Vivo Characterization of Neural Tissue by Dielectric Spectroscopy (DS)." Physiological Measurement 35(2) 195-205

Dobiszewski, Kyle et al. “Design and implementation of a novel superfusion system for ex vivo characterization of neural tissue by dielectric spectroscopy (DS)”, DARPA Neuroscience Engineering, Science, and Technology (NEST) Symposium, San Diego, CA, November, 2010.

“Life isn’t worth living, unless it is lived for someone else”
-Albert Einstein

To the love of my life, Nicole, for your eternal love and support

ACKNOWLEDGMENT

I would like to thank my dissertation co-advisors, Dr. Camelia Prodan and Dr. Andrew Hill, for their continuous and thoughtful guidance and support throughout my education at the New Jersey Institute of Technology. I came to them as an inexperienced undergraduate researcher and, in no small part, due to their constant mentoring during the previous five years, I am leaving them as a published researcher with a broad array of skills and knowledge. I could not ask for anything more in mentors.

I would also like to thank the members of my dissertation committee for all that they have done to mold me into the researcher that I am today. Along with Dr. Prodan, Dr. Gordon Thomas and Dr. Reginald Farrow motivated me to pursue research in the field of biophysics. Their passion for and accomplishment in the field of biophysics provide a model for success that I very much hope to emulate. I would like to thank Dr. Bryan Pfister for all of his guidance and mentoring during both my undergraduate and graduate educations. Dr. Pfister was one of my favorite undergraduate biomedical engineering professors and a catalyst in my decision to pursue a research-based career. Finally, I would like to thank Dr. Alokik Kanwal for his mentoring and willingness to help troubleshoot aspects of my research throughout the years. I feel very blessed to have attracted such a distinguished and diversified dissertation committee; I thank them for their service.

I would like to thank Dr. Fadi Deek for his never-ending guidance, support, and kindness throughout my education at NJIT. It is quite difficult to articulate just how much Dr. Deek has enriched and facilitated my educational pursuits at NJIT but I am

quite confident in saying that I surely would not be where I am today had it not been for Dr. Deek.

So many colleagues have assisted in the success of my research and enriched my education that it would be impossible to acknowledge them all. However, I would like to thank several colleagues that have significantly contributed to my education throughout the last five years. Dr. Corina Bot is a friend, colleague and mentor who was always willing to impart her expansive knowledge on dielectric spectroscopy upon me. Dr. Ashwini Bendiganavale is a friend and colleague that was always been willing to assist me in any aspect of my research. Mr. Matthew Deek is a friend and colleague who was my principal research partner throughout the first half of my graduate studies; he contributed in innumerable ways to the success of the research contained in this dissertation. Mr. Andrew Ghaly was my principal research partner throughout the latter half of my graduate studies. His motivation and knowledge greatly benefited the research presented herein. I would also like to acknowledge Dr. Meldrum Robertson of Queen's University in Ontario, Canada for the assistance that he and his students provided in producing the ion selective electrodes used in the completion of my research.

I would like to sincerely thank the members of my family for their guidance and support, through good times and bad, during my graduate studies. Their contributions to my success have been limitless and I would not be where I have today had it not been for them. Specifically, I would like to thank my father, Mr. Frank Dobiszewski, and my grandfather, Dr. Walter Kraft, for recognizing and nurturing my interest in science and engineering from an early age.

TABLE OF CONTENTS

Chapter	Page
1 INTRODUCTION……..……..…….	1
1.1 Objectives of Research and Questions to Answer……...	1
1.2 Background Information and Review of Relevant Literature……...…...	2
2 THEORY…….	8
2.1 Electrical Properties of Brain Tissue …….……..	8
2.2 Potassium Ion Selective Microelectrodes ……..….	11
3 SUPERFUSION SYSTEM FOR DIELECTRIC SPECTROSCOPY ……...	18
3.1 Background Information……...……...……...….	18
3.2 Methodology Used in Design and Testing……	20
3.3 Results of Testing…….....	26
3.4 Discussion of Results and Conclusions……	30
4 CORRELATING EXTRACELLULAR FLUID CONDUCTIVITY CHANGE WITH INSULT SEVERITY USING DIELECTRIC SPECTROSCOPY……...	32
4.1 Background Information ……...……...…	32
4.2 Methodology……	33
4.3 Results of Conductivity Studies……...	38
4.4 Discussion of Conductivity Studies……	44
4.5 Conclusions …….…...	47
5 MODULATION OF POTASSIUM HOMEOSTASIS BY μ-OPIOID RECEPTOR ACTIVATION DURING SIMULATED ISCHEMIA……...	48

TABLE OF CONTENTS
(Continued)

Chapter	**Page**
5.1 Background Information……...……..……..	48
5.2 Methodology…….……..…….	50
5.3 Results…….…….	60
5.4 Discussion of Results……	64
6 OVERVIEW AND CONCLUDING REMARKS…….…….	67
REFERENCES ……...	69

LIST OF TABLES

Table		Page
2.1	Ion Compositions of Mammalian Intracellular and Extracellular Fluids ….....	9
4.1	Ion Compositions of Experimental Solutions..……..…….	34

LIST OF FIGURES

Figure		Page
2.1	Electrical model of biological tissue……..……..…….	10
2.2	Dielectric permittivity dispersions of tissue……..……..……..……..	11
2.3	Potassium ISM ion migration…….....…..……..	14
2.4	Potassium ISM calibration .....……	16
2.5	Potassium ISM response to varying $[K^+]_O$…..…….……...	17
3.1	Dielectric spectroscopy electrode system..…..……...…	22
3.2	Overview of novel superfusion system……...……	24
3.3	Noise from oxygenation…..……...….	26
3.4	Time Series of conductivity vs. frequency: with and without superfusion……	27
3.5	Conductivity data plotted at 1000 Hz……	28
3.6	Relative dielectric permittivity spectra: with and without superfusion……..	29
4.1	Custom incubation chamber schematic..……	36
4.2	Graph of molar conductivity vs. molar concentration……...…….	39
4.3	Conductivity vs. frequency for different K+ concentrations……..……	40
4.4	Change in extracellular solution conductivity at 100 Hz..……..	41
4.5	Extracellular solution conductivity change as a function of age……...…….	43
5.1	Tip of potassium sensitive microelectrode……...……..	54
5.2	Extracellular population bursting.……..……..	57
5.3	Effect of DAMGO application on bursting frequency……...	60
5.4	DAMGO Dose-Response Curve…….	61

LIST OF FIGURES
(Continued)

Figure		Page
5.5	Correlating potassium concentration change to tonic activity…….……....	61
5.6	Extracellular potassium accumulation during OGD and hypoxia.…….	62
5.7	Effect of DAMGO application during OGD……..……	63

LIST OF ABBREVIATIONS AND SYMBOLS

Na^+	Sodium Ion
K^+	Potassium Ion
Cl^-	Chloride Ion
Ca^{2+}	Calcium Ion
DAMGO	[D-Ala^2, N-MePhe^4, Gly-ol]-enkephalin
K_{ATP}	ATP-gated Potassium Channel
K_{ir}	Inward Rectifying Potassium Chanel
preBötC	Pre-Bötzinger Complex
DS	Dielectric Spectroscopy
MOR	μ-Opioid Receptor
DOR	δ-Opioid Receptor
KOR	κ-Opioid Receptor
OGD	Oxygen-Glucose Deprivation
VRG	Ventral Respiratory Group
ISM	Ion Selective Microelectrode
Δ	Change
$[X]_i$	Intracellular Concentration of Ion X
$[X]_O$	Extracellular Concentration of Ion X
μL	Microliters
° C	Degrees Celcius

mM	Millimolar
mOsm	Milliosmoles
mS	Millisiemens
mV	Millivolts
PDMS	Poly(dimethylsiloxane)
PVC	Poly(vinyl chloride)
EU	European Union
Z	Impedance
ATP	Adenosine Triphosphate
$\mathbf{Re}\{\lvert Z\rvert\}$	Real Component of Z
$\mathbf{Im}\{\lvert Z\rvert\}$	Imaginary Component of Z
ABS	Acylonitrile Butadiene Styrene
Hz	Hertz
kHz	Kilohertz
ANOVA	Analysis of Variance
Λ	Molar Conductivity
aCSF	Artificial Cerebrospinal Fluid
V_m	Membrane Voltage
R	Universal Gas Constant
T	Temperature
Z	Valence
F	Faraday's Constant
P_X	Permeability of Ion X

min	Minutes
ω	Angular Frequency
C	Capacitance
R	Resistance
d	Distance Between Two Points
A	Area
σ	Conductivity
ε	Permittivity
ε_0	Permittivity of Free Space
R_m	Membrane Resistance
R_f	Fluid Resistance
C_m	Membrane Capacitance
U	Internal Energy
Q	Heat
W	Work
P	Pressure
V	Volume; Voltage
S	Entropy
G	Gibb's Free Energy; Gauge
CSF	Cerebrospinal Fluid
n	Number of Molecules; Moles
μ	Chemical Potential

E	Electrical Potential
MHz	Megahertz
α_i	Activity of Molecule i
c_i	Concentration of Molecule i
γ_i	Activity Coefficient of i
O_2	Gaseous Oxygen
q	Charge
$\bar{\mu}_i$	Electrochemical Potential of Molecule i
EC_{50}	Fifty Percent Effective Concentration
N_2	Gaseous Nitrogen
CO_2	Gaseous Carbon Dioxide

CHAPTER 1

INTRODUCTION

In this introductory chapter, the objectives of the three related projects that comprise this dissertation are outlined and a brief review of literature relevant to the topics discussed herein is offered. The second chapter provides a theoretical basis for the two main electrophysiology characterization techniques (dielectric spectroscopy (DS) and potassium sensitive microelectrodes) utilized in this research. The third, fourth, and fifth chapters provide full accounts of the methodology and relevant results of the three related projects that comprise this dissertation. In addition to brief literature review offered in the present chapter, Chapters 3,4, and 5 open with an in-depth introduction and review of relevant literature. The work outline in Chapters 3 and 4 has previously been published (Dobiszewski *et al.*, 2012; Dobiszewski *et al.*, 2011).

1.1 Objectives of Research and Questions to Answer

The objective of this dissertation is to present three distinct, yet related, projects that investigate the flow of ions and other charged particles into or out of brain tissue based on a number of different parameters and circumstances. Specifically, the research contained herein examines and answers the following questions:

1. How does the flows of various ions and other charged particles affect the electrochemical characterization of the tissue by dielectric spectroscopy (DS) and how can this effect be accounted for?
2. Can the change in conductivity of the extracellular fluid as a function of neural insult severity provide insight into the health of the tissue?
3. Does pharmacological manipulation of the μ-opioid receptor attenuate the accumulation of extracellular potassium during oxygen glucose deprivation (OGD)?

1.2 Background Information and Review of Relevant Literature

The mammalian circulatory system consists of miles upon miles of blood vessels that carry blood that has a high concentration of oxygen and nutrients to the cells while carrying the byproducts of cellular respiration from the cells. While at rest, approximately 20% of the oxygen within the blood is routed to the brain (Kety, 1957). When the blood vessels in the brain become occluded, thus depriving the neural tissue of this oxygen and nutrients, ischemic stroke occurs. Ischemic stroke is a leading cause of mortality and morbidity; it kills approximately 130,000 Americans every year (Kochanek *et al.*, 2012). These statistics are of profound interest to an experimental neuroscientist because they prove that catastrophic damage occurs to neural tissue when it is deprived of oxygen and nutrients.

During *in vitro* experimentation, the intrinsic ability of the studied organ to provide for its own supply of oxygen and nutrients is often compromised by experimental design. Therefore, in order to combat the deterioration of tissue with time, supplying oxygen and nutrients is appropriate (Hajos and Mody, 2009). Two related methods are utilized to provide oxygen and nutrients to the tissue being studied: superfusion and perfusion. Perfusion makes use of an external pump along with the tissue's own blood vessels to supply the cells with a solution rich in dissolved oxygen and nutrients. Superfusion utilizes an external pump and plumbing network to bathe the tissue sample in solution rich in oxygen and nutrients. The importance of perfusion and superfusion cannot be understated. In fact, ischemia can be simulated *in vitro* by simply discontinuing use of the external pump used to supply oxygen and nutrient rich solution to the tissue (Morawietz *et al.*, 1995).

Several techniques including patch clamping, imaging with voltage-sensitive dyes, ion selective electrodes and dielectric/impedance spectroscopy, are currently utilized by

researchers to quantify the electrophysiological properties of a system. Among these techniques, dielectric spectroscopy (DS) has emerged as a powerful method for characterizing biological systems(Schwan, 1957; Gheorghiu, 1993; Prodan *et al.*, 2004). In fact, DS has been used to investigate a variety of cellular and tissue properties, such as membrane potential (Bot and Prodan, 2009), membrane structure and properties (Gheorghiu and Gersing, 2002; Di Biasio and Cametti, 2011; Ron *et al.*, 2008), glucose concentration in tissue (Caduff *et al.*, 2006), and to distinguish between the different cellular death mechanisms (Lee *et al.*, 2009). Furthermore the dielectric properties of a biological system are closely related to the overall health of that system (Gheorghiu, 1996).

While a number of different custom superfusion apparatus intended for application-specific measurements of neural function (Yamamoto and McIlwain, 1966; White *et al.*, 1978; Alger and Nicoll, 1981) have been described, a search of the relevant scientific literature revealed no examples of superfusion systems designed for use with DS. This revelation is surprising considering the robust applications of DS in biophysics and electrophysiology. In fact, while the large databases of various dielectric properties for nearly every major mammalian organ system (Gabriel *et al.*, 1996; Gabriel, 2007), provides a wealth of knowledge, they contain data almost exclusively collected from excised tissue. Therefore, observed changes in these data do not necessarily correspond to changes in any physiological variables within the system (Foster and Schwan, 1996).

The classical experiments of Hodgkin and Huxley provide an explanation of how the flow of ions results in the bioelectric signaling (Hodgkin and Huxley, 1952). The ability of neural cells to regulate this flow of ions and thus create ionic gradients is paramount for a stable cellular membrane potential (Kettenmann *et al.*, 1983; Hodgkin and Keynes, 1955)

and the viability of neurons (Husted and Reed, 1977). Accordingly, drastic changes in membrane potential due to ionic fluctuations can have devastating effects on signaling. Therefore, ionic homeostasis dysfunction and resulting electrophysiological changes are indicative of a number of different common pathological condition, including hypoxia/ischemia (Murai *et al.*, 1997; Müller and Somjen, 2000; Hansen, 1985; Hansen and Nedergaard, 1988), traumatic head injury (Takahashi *et al.*, 1981; Santhakumar *et al.*, 2003), neurodegeneration (Hartley *et al.*, 1999; Ye *et al.*, 2004), and epilepsy (Fröhlich *et al.*, 2008). Ionic homeostasis dysfunction is known to be damaging and ionic efflux from cells precedes the cellular death mechanisms of necrosis and apoptosis (Bortner *et al.*, 1997; Warny and Kelly, 1998; Remillard and Yuan, 2004).

Of particular interest to the research contained within this dissertation is the change in ion homeostasis dysfunction that accompanies hypoxic and ischemic insults. This dysfunction is characterized by increases in intracellular concentrations of sodium, chloride, calcium and increases in the extracellular concentrations of hydrogen and potassium (Haddad and Yao, 2004; Jiang *et al.*, 1992; Hansen, 1985; Hansen and Nedergaard, 1988). This shift in ion concentrations is correlated with a sudden depolarization (Müller and Somjen, 2000). Of all the ion concentration changes, potassium stands out in that it is the only one that occurs in a biphasic manner. Phase one of extracellular potassium accumulation involves a sudden, modest increase, followed several minutes later by phase two, which involves a punctuated and profound increase (Hansen and Nedergaard, 1988). Changes in concentration of other ions correspond temporally to phase two (Hansen, 1985).

Under normal conditions, it is believed that astrocytes are chiefly responsible for the maintenance of extracellular potassium (Walz, 2000). These glia contain a specific inwardly

rectifying potassium channel ($K_{ir}4.1$) that aids in the buffering of extracellular potassium (Higashi *et al.*, 2001; Neusch *et al.*, 2006). In addition to K_{ir} channels, the Na^+/K^+ ATPase contributes to extracellular potassium regulation. (D'Ambrosio *et al.*, 2001). Interestingly, K_{ir} channels display behavior in that deviates from that predicted by the Hodgkin-Huxley kinetics in that they show greater inward flow of potassium than outward flow (Hibino *et al.*, 2010). One K_{ir} channel subunit, known as K_{ATP}, is gated by intracellular ATP levels (Craig *et al.*, 2008), thus directly linking membrane potassium permeability to metabolism. Research has been shown that K_{ATP} channels confer protection upon neural tissue during episodes of hypoxia (Ballanyi, 2004) and epilepsy (Yamada and Inagaki, 2005). Of note, both of these conditions are related to extracellular potassium accumulation.

It is well documented that the increase in extracellular potassium concentration is responsible for cellular death (Yu *et al.*, 1999; Remillard and Yuan, 2004; Liu *et al.*, 2003). This statement is particularly relevant in hypoxia/ischemia, where potassium efflux is directly related to cellular death (Liu *et al.*, 2003) and potassium channel blockers attenuate this death (Wei *et al.*, 2003). The turtle, which is often environmentally deprived of oxygen, has adapted special mechanisms to protect against anoxic damage. These protective mechanisms result in far less extracellular potassium accumulation, compared to mammalian tissue (Xia *et al.*, 1992; Sick *et al.*, 1982). It appears that these protective mechanisms relate to the attenuation of excitotoxicity (Pamenter *et al.*, 2008). It is interesting to note that the turtle cortex contains an extremely high density of δ-opioid receptors (DOR) (Xia and Haddad, 2001) and their antagonism abolishes the aforementioned protective mechanisms (Pamenter and Buck, 2008).

Opioids are a class of neuropeptides belonging to the G protein-coupled receptor

family (Raynor *et al.*, 1994) that have been shown to have modulatory effects on potassium (Ikeda *et al.*, 1995), calcium (Su *et al.*, 1998; Toselli *et al.*, 1997), chloride (Kromer, 1993) and sodium (Witkowski and Szulczyk, 2006) currents. The three known opioid receptors sub-types are the μ, δ, and κ (MOR, DOR, and KOR, respectively); they have been found to be widely distributed throughout the mammalian nervous system (Goodman *et al.*, 1980). While these receptors are distinctly different, they have been shown to have common effects on several ion channels and currents (Toselli *et al.*, 1997). Evidence suggests that DOR activation during oxygen-glucose deprivation (OGD; simulated ischemia) in the rat cortex attenuates the accumulation of extracellular potassium (Chao *et al.*, 2007b; Chao *et al.*, 2012; Chao and Xia, 2010) through the inhibition of sodium and calcium influx (Chao *et al.*, 2008; Chao *et al.*, 2007a; Chao *et al.*, 2012; Kang *et al.*, 2009), thus protecting neural tissue from injury and death (Zhang *et al.*, 2002). Interestingly, MOR activation did not show the same capability to modulate potassium homeostasis dysfunction during OGD in the cortex (Chao *et al.*, 2007a).

The Pre-Bötzinger Complex (preBötC) is a region of the brainstem within the ventral respiratory group (VRG) that is responsible for respiratory rhythm generation (Smith *et al.*, 1991). The preBötC is also sensitive to acute changes in oxygen concentration in that it acts as a hypoxic chemoreceptor for respiratory function (Solomon *et al.*, 2000). In order for neural cells to be characterized as oxygen sensitive, the following criteria must be met (Teppema and Dahan, 2010):

- The hypoxia-induced depolarization must occur independent of synaptic transmission,
- Activation is independent of arterial chemoreceptor input.
- During normoxic conditions, the sensitivity of these cells should be greater than that of other neurons.

- During hypoxic conditions, a response, in the form of respiratory modulation, is elicited.

When deprived of oxygen the frequency of the respiratory rhythm generated from the preBötC initially increases and then eventually decreases (Ballanyi and Richter, 1995).

CHAPTER 2

THEORY

In Chapter 2, the theoretical basis for the experimental procedures that are presented in this dissertation are outlined and reviewed. Specifically, the electrical properties of tissue are examined, with emphasis on how these electrical properties relate to characterization by dielectric spectroscopy. Additionally, the Nernst equation is derived from thermodynamic principles and related to the function of potassium selective microelectrodes.

2.1 Electrical Properties of Brain Tissue

In 1836, the English physicist Michael Faraday discovered the concept of the electric field when he placed a voltage generator in a metal enclosure (Faraday cage). Faraday observed that the resulting electric field lines passed through certain materials that were not carrying electricity. To help describe such materials, Faraday turned to fellow Englishman William Whewell, who combined the words "dia" (Greek for through) and "electric" to coin the term dielectric. Dielectric spectroscopy, also known as impedance spectroscopy, is a materials characterization technique that investigates the interaction between an external electric field and the polarizability of a material by measuring that material's impedance as a function of frequency. Impedance is defined as a material's ability to resist the flow of alternating current; it is a complex function that can be comprised of resistive, capacitive and inductive components.

Biological cells are defined by the boundaries of their plasma membrane, which separates the extracellular fluid from the intracellular cytosol; both the extracellular fluid and the intracellular cytosol are highly electrolytic but with different ionic profiles. The approximate ionic composition of these fluids in mammalian neural tissue is presented in Table 2.1:

Table 2.1 Ion Compositions of Mammalian Intracellular and Extracellular Fluids

Ion	**Intracellular Concentration** (mM)	**Extracellular Concentration** (mM)
Sodium	5-15	145
Chloride	4-30	110
Calcium	0.0001	1-2
Potassium	140	5

Source: (Purves *et al.*, 2008)

These ions contribute to the resting membrane potential according to the Goldman equation:

$$V = \frac{RT}{zF} \ln \frac{P_K[K]_O + P_{Na}[Na]_O + P_{Cl}[Cl]_O}{P_K[K]_i + P_{Na}[Na]_i + P_{Cl}[Cl]_i} \quad (2.1)$$

The membrane consists of a phospholipid bilayer that is sprinkled with a plethora of transmembrane macromolecules, such as ion channels, pores, and junctions. The passive electrical properties of this heterogeneous system are defined by both its resistive (transmembrane macromolecules) and capacitive components (phospholipids). Due to the spatial orientation of these components within the system, a parallel RC configuration most accurately describes the equivalent electrical model of the membrane (Varghese, 2000). Because this configuration consists of both reactive and elements (Figure 2.1), the impedance is described by the following complex function:

$$\frac{1}{Z} = \frac{1}{Z} + i\,\omega C \tag{2.2}$$

Through algebraic manipulation and application of a complex conjugate, this relationship can be expressed as:

$$Z = \frac{d\sigma + i\omega d\varepsilon_0 \varepsilon}{\sigma^2 A + \omega^2 \varepsilon_0^2 \varepsilon^2 A} \tag{2.3}$$

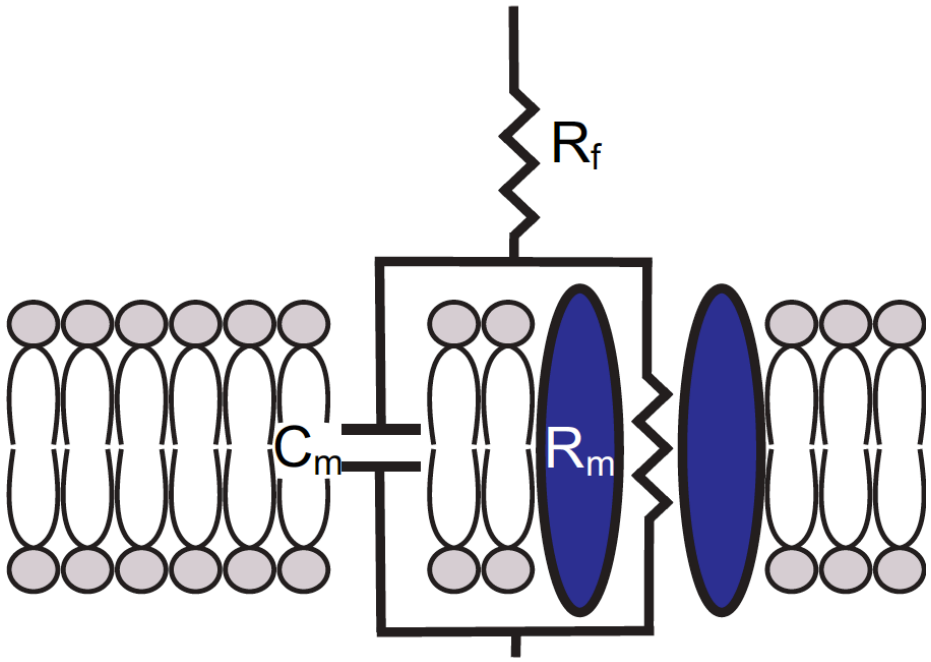

Figure 2.1 Electrically, brain tissue can be modeled as a parallel RC circuit in series with a resistor. The C_m component represents the capacitive properties of the phospholipids while the R_m and R_f components represent the resistive properties of the transmembrane proteins and the intracellular and extracellular fluid, respectively.

When a resistive component representing the intracellular and extracellular fluids is added in series to the parallel RC circuit (As seen in Figure 2.1), the impedance equation becomes:

$$Z = R_f + \frac{d\sigma + i\omega d\varepsilon_0 \varepsilon}{\sigma^2 A + \omega^2 \varepsilon_0^2 \varepsilon^2 A} \tag{2.4}$$

Due to its intrinsic electrical properties, biological tissue displays a distinctive

frequency response, in the form of a number of different dispersions (Figure 2.2). These dispersions are the result of the interaction of the applied electrical field to the various components of the tissue. The α dispersion results from the tangential flow of ions across the cell membrane, the β dispersion results from the build-up of charge at the cell membrane, the δ dispersion results from rotation of macromolecule side-chain and water molecules, and the γ dispersion results from the dipolar rotation of water molecules (Markx and Davey, 1999).

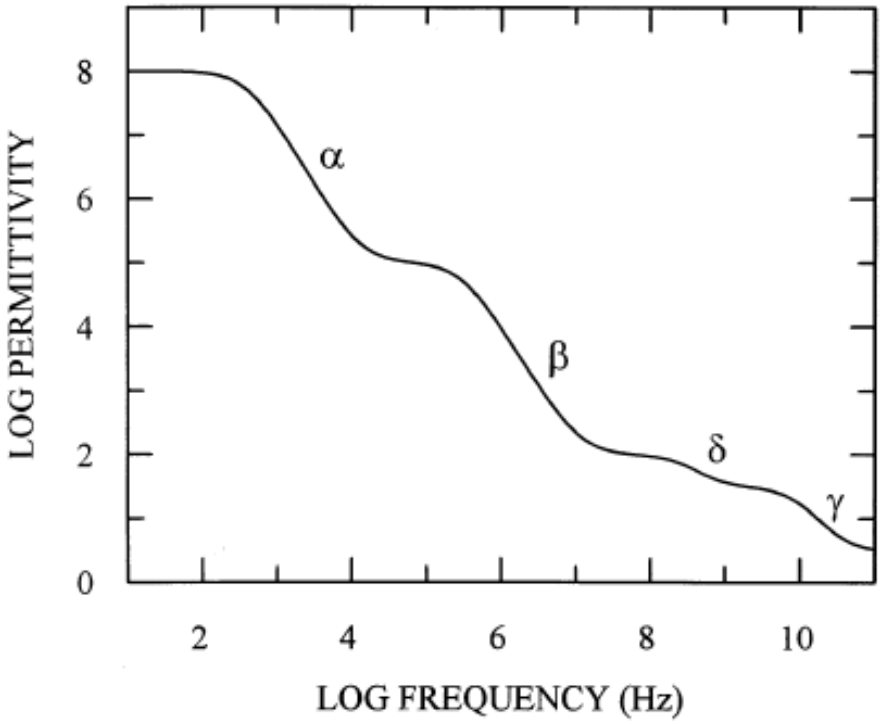

Figure 2.2 The characteristic frequency response of biological tissue in the form of the α, β, δ, and γ dispersions.

Source: (Markx and Davey, 1999)

2.2 Potassium Ion Selective Microelectrodes

The theoretical basis of ion selective electrode function rests in the Nernst equation. In order to be responsive to an individual ion, all ion selective electrodes consist of a membrane layer

that is far more permeable to that ion over all others in solution. That ion moves through the membrane and along its concentration gradient, thus inducing an electrical potential. This net movement of ions only stop when that electrical potential can equivalently counteract the chemical potential of the concentration gradient. Equilibrium thermodynamics dictates the circumstances under which such conditions are met.

The First Law of Thermodynamics states that $dU = dQ + dW$ while the Second Law of Thermodynamics states that $dS = dQ/T$ when a reversible process occurs in a closed system. These laws can be algebraically manipulated to produce the relationship $dU = TdS + dW$. The work differential (dW) can be considered the summation of all the different sources of work that can be done on or by the system. Among others, these sources include the relationship between pressure and volume ($dW_{pV} = -pdV$), number of molecules and chemical potential ($dW_{n\mu} = \mu dn$), and between charge and electrical potential ($dW_{qE} = Edq$). If only these sources of work are considered, the work differential becomes:

$$dW = dW_{pV} + dW_{n\mu} + dW_{qE} = -pdV + \mu dn + Edq \tag{2.5}$$

If more than one type of molecule occupies the system, the $W_{n\mu}$ term must be expanded to reflect this fact. Accordingly, for a system containing n different molecules:

$$dW_{n\mu} = \sum_{i=1}^{n} \mu_i dn_i \tag{2.6}$$

Thus, the Gibb's Fundamental Equation is formed from these relationships:

$$dU = TdS - pdV + \sum_{i=1}^{m} \mu_i dn_i + Edq \tag{2.6}$$

From this relationship, the chemical potential of a molecule is defined, with respect to activity (α_i), as:

$$\mu_i = \left(\frac{\partial U}{\partial n_i}\right)_{S,V,q} = \mu_i^0 + RTln\alpha_i \tag{2.7}$$

The relationship between concentration *(c_i)* and activity is $\alpha_i = \gamma_i c_i$ where γ_i is the activity coefficient of the ion in solution. Debye and Hückel (Debye and Hückel, 1923) described the relationship between concentration and the activity function in dilute solutions as:

$$\log \gamma_i = -Az_i^2\sqrt{c_i} \tag{2.8}$$

Where A is a solvent and temperature-dependent constant that is computed using the following equation:

$$\mathrm{A} = \frac{1.8246 \text{ x } 10^6}{(\varepsilon \mathrm{T})^{3/2}} \tag{2.9}$$

The charge (q) of a single ion with charge z can be expressed in terms of Faraday's constant (F) and moles (n) as q= *z*nF; the differential of this relationship is $d\mathrm{q} = z\mathrm{F}d\mathrm{n}$. Again, assuming the system consists of *n* different ions, this relationship can be expressed as:

$$d\mathrm{q} = \sum_{i=1}^{n} z_i \mathrm{F} d\mathrm{n}_i \tag{2.10}$$

Returning to the Gibb's Fundamental Equation and taking into account these relationships yields:

$$d\mathrm{U} = \mathrm{T}dS - \mathrm{p}d\mathrm{V} + \sum_{i=1}^{m} \mu_i d\mathrm{n}_i + \mathrm{E} \sum_{i=1}^{m} z_i \mathrm{F} d\mathrm{n}_i \tag{2.11}$$

Combining like terms ($d\mathrm{n}_i$) results in:

$$d\mathrm{U} = \mathrm{T}dS - \mathrm{p}d\mathrm{V} + \sum_{i=1}^{m} (\mu_i + z_i \mathrm{F})\, d\mathrm{n}_i \tag{2.12}$$

The expression in parentheses in the final term of this simplified version of Gibb's Fundamental Equation is the electrochemical potential ($\overline{\boldsymbol{\mu}}_{\boldsymbol{i}}$) of the ion. This electrochemical

potential is used in the derivation of the Nernst Equation in that a state of equilibrium exists between the electrochemical potentials of an ion separated by a semipermeable membrane on each side of that membrane. In the case of the potassium ion selective electrodes, there are potassium (K^+) and chloride (Cl^-) ions that are dissociated (completely) in solution on each side of the semipermeable membrane (valinomycin), as depicted in the Figure 2.3.

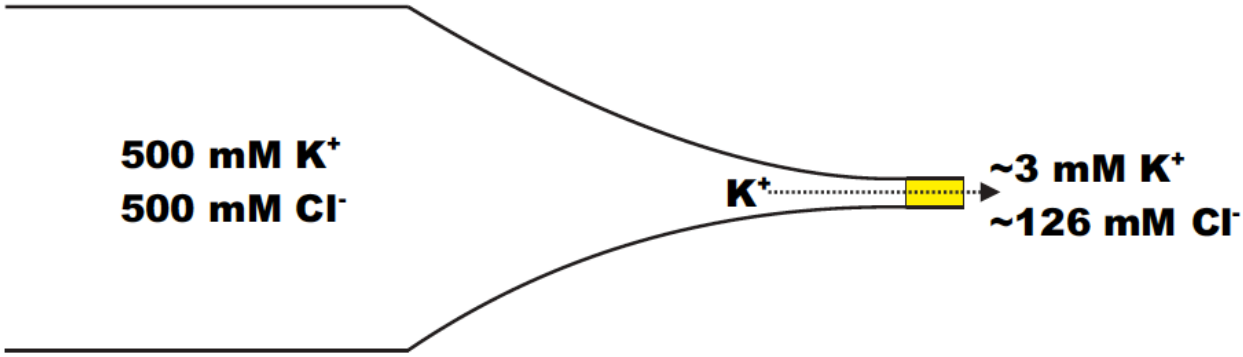

Figure 2.3 Schematic of the potassium and chloride ion concentrations on both sides of the ionophore membrane (yellow). The valinomycin within the ionophore membrane allows the passage of the potassium ions while denying the passage of the chloride ions. The migration of potassium ions from interior to the exterior of the electrode continues until the electrochemical potentials are in a state of equilibrium. This selective movement of ions and the resulting potential are the theoretical basis for ion selective electrode function.

Valinomycin is a cyclic depsipeptide that is derived from the *Streptomyces fulvissimus* microbe that was first described by Brockmann and Schmidt-Kastner (Brockmann and Schmidt-Kastner, 1955). It is a natural ionophore that is highly selective for potassium over other ions (Tosteson *et al.*, 1967). Since valinomycin is permeable to potassium, but not chloride, potassium will flow along its concentration gradient, thus leading to a disturbance of the electrostatic equilibrium of the system. Potassium will move along its concentration gradient until the potential difference that is created by this movement becomes great enough to hinder further diffusion of potassium; at this point, the potassium's electrochemical potentials on each side of the membrane are in a state of

equilibrium:

$$\overline{\boldsymbol{\mu}}_{K+}^{in} = \overline{\boldsymbol{\mu}}_{K+}^{out} \tag{2.13}$$

$$\mu_{\mathrm{K+}}^{0,\mathrm{in}} + \mathrm{RT}^{\mathrm{in}} \ln \alpha_{\mathrm{K+}}^{\mathrm{in}} + \mathrm{zFE}^{\mathrm{in}} = \mu_{\mathrm{K+}}^{0,\mathrm{out}} + \mathrm{RT}^{\mathrm{out}} \ln \alpha_{\mathrm{K+}}^{\mathrm{out}} + \mathrm{zFE}^{\mathrm{out}} \tag{2.14}$$

The charge on a potassium ion is +1, so z=1. Furthermore, since the temperature is rigorously controlled throughout the course of the experiment with little fluctuations, $T^{out}=T^{in}=T$ and since the experiment is performed at atmospheric pressure throughout, the pressure differential is zero and $\mu_{\mathrm{K+}}^{0,\mathrm{out}} = \mu_{\mathrm{K+}}^{0,\mathrm{in}}$. Based on this knowledge and these assumptions:

$$\mathrm{F}(\Delta \mathrm{E}) = \mathrm{RT}(\ln \alpha_{\mathrm{K+}}^{\mathrm{out}} - \ln \alpha_{\mathrm{K+}}^{\mathrm{in}}) \tag{2.15}$$

Rearranging this equation and substituting concentration for its relative activity yield the familiar Nernst equation for the potassium ion:

$$\Delta \mathrm{E} = \frac{\mathrm{RT}}{\mathrm{F}} \ln \frac{[\mathrm{K}^+]_{\mathrm{out}}}{[\mathrm{K}^+]_{\mathrm{in}}} \tag{2.16}$$

Based on this equation and a two-point calibration over a decade change in concentration, an expression can be derived that relates voltage (obtained experimentally) to extracellular potassium concentration. To do this conversion, modify the Nernst equation from its natural logarithm form to its logarithm form by multiplying by 2.303. Also, adjust the nomenclature such that $[\mathrm{K}^+]_{\mathrm{in}}$ corresponds to some initial known potassium concentration ($[\mathrm{K}^+]_1$) and $[\mathrm{K}^+]_{\mathrm{out}}$ corresponds to a second known potassium concentration ($[\mathrm{K}^+]_2$) such that $[\mathrm{K}^+]_2 = 10[\mathrm{K}^+]_1$. Figure 2.4 shows such the potential change when the

potassium concentration of artificial cerebrospinal fluid was increased from 3 mM to 30 mM:

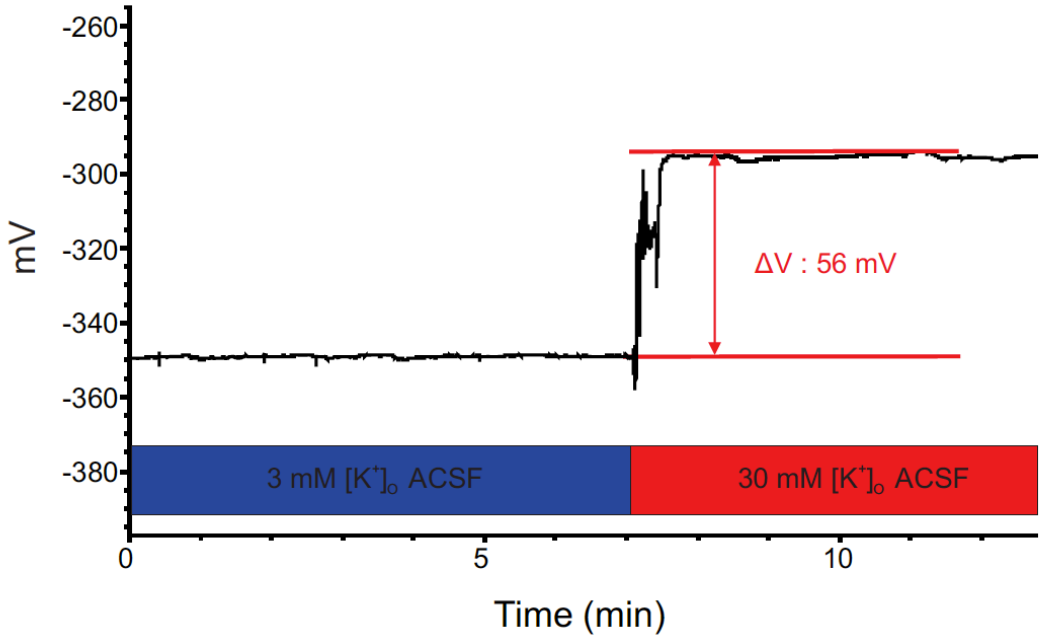

Figure 2.4 In this calibration experiment in which the extracellular concentration of potassium was altered from 3 mM to 30 mM, the potassium selective microelectrode displayed a reasonable change in voltage based on the Nernst equation.

Since the change in concentration of K^+ was tenfold in the above example, the Nernst equation becomes:

$$\Delta E = \frac{2.303\ RT}{F} \log \frac{[K^+]_2}{[K^+]_1} = \frac{2.303\ RT}{F} \log \frac{10[K^+]_1}{[K^+]_1} = \frac{2.303\ RT}{F} \tag{2.17}$$

Assuming temperature is controlled experimentally at 32° C, this value becomes 0.0605 J/C (using the conversion 1 J/C = 1000 mV), ΔE=60.5 mV for this change in concentration. However, as seen in the Figure 2.2, the experimental change in potential is slightly less than the expected value from the Nernst equation. There are several possible explanations for this discrepancy. The most plausible explanation is because concentration was indiscriminately

substituted for activity in the above calculations. If the activity was indeed utilized, the expected change in potential would be 57.1 mV, assuming the solvent was cerebrospinal fluid with a dielectric constant of 79.47 (Penn and Bell, 1978). Another possible explanation for the slightly lower-than-expected change in potential involves the use of AgCl as a reference electrode (Mohan and Bates, 1975). The experimental change in potential for the decade change in concentration (ΔV) is then used to convert voltage to concentration. To do so, the voltage signal must be "zeroed" at the lower of the two calibration concentrations such that any experimental change in potential is calculated from this "zeroed" point $\Delta E = (E_{experimental} - E_{[K+]1})$. The following equation (2.18) can then be used to find an experimental potassium concentration:

$$[K^+]_{experimental} = [K^+]_1 * 10^{\Delta E/\Delta V} \quad (2.18)$$

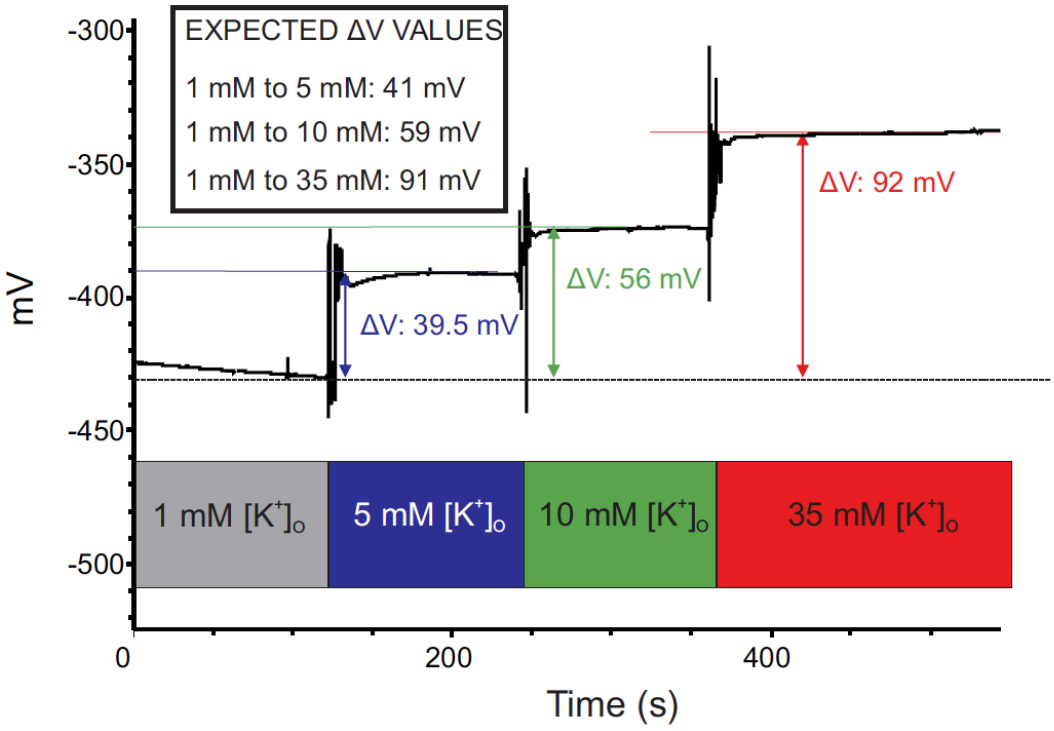

Figure 2.5 The actual voltage response of the potassium selective microelectrodes to varying potassium concentrations closely mirrored the expected responses, based on Eq. 2.18.

CHAPTER 3

SUPERFUSION SYSTEM FOR DIELECTRIC SPECTROSCOPY

3.1 Background Information

The emerging field of electrophysiology encompasses the study of a biological system's intrinsic electrical properties. One of the primary biological signaling mechanisms is the action potential, which is an electrical potential difference generated by the mammalian nervous system. Therefore, the study of mammalian neural systems is intimately contingent upon and portrayed by various electrophysiological properties. Several techniques, including patch clamping, imaging with voltage-sensitive dyes, and dielectric/impedance spectroscopy, are currently utilized by researchers to quantify the electrophysiological properties of a biological system. Among these techniques, dielectric spectroscopy has emerged as a powerful method for characterizing biological systems (Schwan, 1957; Gheorghiu, 1993; Prodan *et al.*, 2004). Various alterations the electrical properties of a neural systems have been implicated in a number of common pathologies, including neurodegeneration (Hartley *et al.*, 1999; Ye *et al.*, 2004) and cerebral concussion (Gennarelli, 1986) as well as several less common pathologies such as blepharospasm and oromandibular dystonia (Berardelli *et al.*, 1985).

The dielectric properties of a biological system, as obtained by dielectric spectroscopy, are closely related to the overall health of that system (Gheorghiu, 1996). Citing this relationship, researchers began studying the dielectric properties of excised tissue as early as the 1930's. While some dielectric spectroscopy measurements have been taken *in vivo,* the majority of tabulated data regarding the dielectric properties of tissue comes from

excised tissue far removed from physiological conditions (Foster and Schwan, 1996). Gabriel and Gabriel provide a database of various dielectric properties for nearly every major mammalian organ system while concurrently offering an excellent overview into researchers' current understanding of the dielectric properties of biological tissue (Gabriel *et al.*, 1996; Gabriel, 2007). While this database provides a wealth of knowledge, it is populated almost solely by data collected from excised tissue. Therefore, as noted by Foster and Schwan (1996), changes in the dielectric properties observed in these data do not necessarily correspond to direct changes in any physiological variables within the system.

Therefore, a novel superfusion system was designed to increase the correlation of data obtained *in vitro* from excised neural tissue to the *in vivo* dielectric properties of biological tissue. The system increases this correlation by continuously providing a single slice of cortical tissue with ample nutrients (in this case, glucose) and oxygen for *ex vivo* measurements. While this superfusion design is applicable to any tissue sample, the authors' desire to investigate the dielectric properties of neural tissue necessitated the use of such a system. The mammalian nervous system is a very metabolically active organ system, with the human brain being responsible for approximately 20% of resting oxygen consumption (Kety, 1957).

Henry McIlwain was one of the earliest pioneers in brain slice preparations and subsequent efforts to maintain excised tissue viability by superfusion (Collingridge, 1995). The earliest superfusion chambers were custom-made apparatus intended for application-specific measurements of neural function (Yamamoto and McIlwain, 1966; White *et al.*, 1978; Alger and Nicoll, 1981). These early systems proved capable of maintaining *in vitro* neural tissue viability for up to twelve hours by use of superfusion (Haas *et al.*, 1979). These

same superfusion systems gave way to commercial apparatus such as the Coleman superfusion bath system (Harvard Apparatus; Holliston, Massachusetts). While a wide diversity of superfusion system designs have been described in literature, the authors thus far have been unable to discover a system solely intended for use with dielectric spectroscopy. The system presented here is similar to previously described apparatuses in that it provides oxygen and nutrient-rich extracellular solution to the tissue while providing features similar to other systems such as the ability to rapidly change between two experimental solutions. However, this apparatus differs from previously described superfusion systems in that it was designed such that it could function during dielectric spectroscopy characterization of neural tissue slice preparations without adversely affecting the measurement.

3.2 Methodology Used in Design and Testing

3.2.1 Design of Electrode System

The integral component of the superfusion system is the custom designed electrode array as shown in Figure 3.1. This general design has previously been shown to measure accurate values of the complex dielectric permittivity of a variety of materials (Bot and Prodan, 2009; Dobiszewski *et al.*, 2012; Dobiszewski *et al.*, 2011; Prodan and Bot, 2009; Prodan *et al.*, 2004). At the core of this parallel plate electrode array are two solid 14-karat white gold electrodes of 10.8 mm diameter. Solid gold was chosen for the electrode material with consideration to its low resistivity and to its cathodic nature. The inert properties of the gold minimize reactions with the strong electrolytic solutions as the electrode-solution interface.

The electrodes are enclosed in a clear polyvinyl chloride (PVC) pipe (ALSCO Industrial Products, Inc. Lithia Springs, GA 30122) with inner diameter of 12 mm cut to a

length of 76 mm. The diameter of the upper and lower electrodes was sized approximately 1 mm smaller than the inner diameter of the PVC tube enclosure. This sizing reduces error caused by stray capacitance at the edge of the electrodes. Specifically, error was reduced by encouraging stray electric field lines to travel through either the PVC tube enclosure or the air. Since the dielectric permittivity of both these materials is much lower than that of the electrolytic solution, the contribution of the stray capacitance on the overall measurement is minimized.

The separation distance between the electrodes was precisely controlled by a metric micrometer head with non-rotating spindle (Mitutoyo Part # 153-101). The majority of the structural members and couplings of the electrode array (grey parts in Figures 3.1 and 3.2) were produced from acylonitrile butadiene styrene (ABS) thermoplastic via the Dimension Elite Series three dimensional printer/rapid prototype (Stratasys Inc. Eden Prairie, MN 55344). The structural members were linked together and secured by 10-32 acetyl threaded rods and associated hardware (McMaster-Carr; Robbinsville, NJ 08691-2343).

This apparatus was previously proven to measure accurately the dielectric permittivity of different liquids with known values from 4 to 78 (Bot and Prodan, 2009; Prodan and Bot, 2009; Prodan *et al.*, 2004).

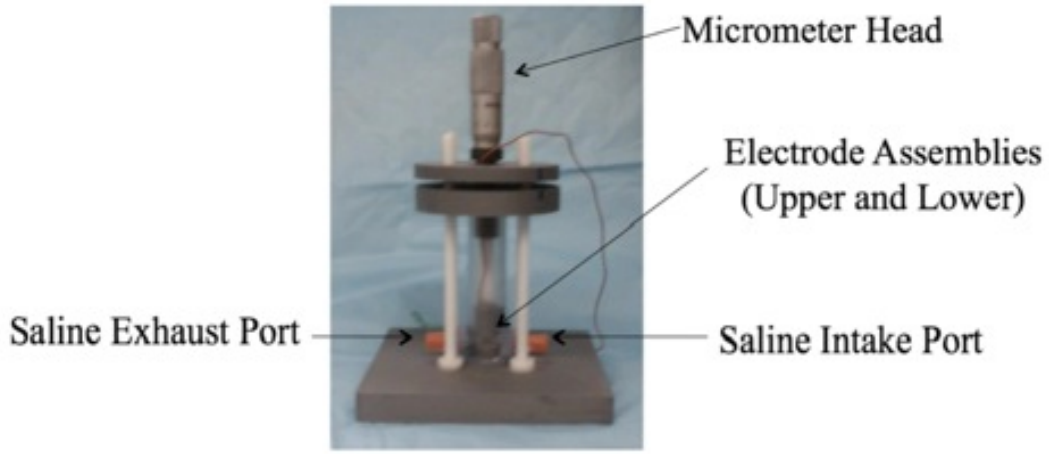

Figure 3.1 Image of the custom parallel plate electrode array designed and built by the authors. The grey members in the image are comprised of ABS thermoplastic and were produced using the rapid prototyping technology. The electrode material is 14K white gold due to its cathodic (inert) properties as well as its low resistivity. A metric micrometer head precisely controls the separation distance between the electrodes.

3.2.2 Design of Superfusion System

The tissue sample lies between the mobile upper electrode assembly and the stationary lower electrode. The volume between the electrodes is the only spatial region within the apparatus that must strictly mimic physiological conditions. The superfusion system was designed to provide the maximum volume of nutrient-rich and oxygen-saturated electrolytic fluid to the spatial region containing the tissue during characterization. Therefore, two 3/16 inch transverse holes were drilled through the PVC enclosure at 180 degrees of separation at such a height that the holes would be flush with the lower electrode. The directions of the holes were parallel to the plane of the electrode. Two 14 gauge fluorinated ethylene-propylene (FEP) intravenous (IV) catheters with female Leur lock connections were cut to a length of 2.8 mm to correspond to the schedule 40 classification of the PVC pipe. The end of the catheter was inserted through the transverse holes such that the end of the catheter was flush with the inner wall of the PVC enclosure.

As schematically portrayed in Figure 3.2, one catheter serves as the intake port for the nutrient/oxygen-rich solution, which is fed to the tissue-containing compartment through a gravity-fed design whereby a 60 mL syringe serves as the electrolyte reservoir and semi-rigid tubing served as the conduit from the reservoir to the intake port. The reservoir was positioned at such a height that the vertical distance between the solution level and the intake port was 120 mm. Solution was continuously added to the reservoir to maintain this 120 mm height. The height of the solution coupled with the inner diameter (1.67 mm) and length (80 mm) of the semi-rigid tubing resulted in an electrolyte flow rate into the chamber of approximately 6 mL/minute; this flow rate is considered adequate for tissue survivability (Hajos and Mody, 2009). Oxygenation of the experimental electrolytic solution must occur prior to the addition of the solution to the syringe reservoir. Therefore, in order to ensure total oxygen saturation as closely as possible, the top of both the 60 mL reservoir and the larger saline storage container in which oxygenation actually occurs is enclosed. Oxygenation via air stone bubbling directly in the 60 mL reservoir leads to a variety of noise errors associated with the formation of oxygen-filled bubbles between the electrodes. Since the relative dielectric permittivity of oxygen is different from that of neural tissue and electrolytic solution, the contribution of the oxygen bubbles are quite apparent, as described later in this chapter.

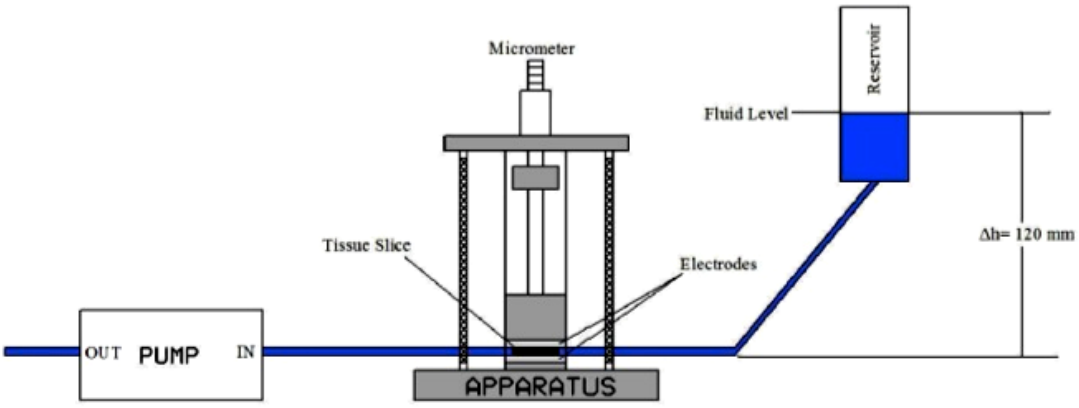

Figure 3.2 The key aspects of the novel superfusion system are the custom-designed and built gold electrode array, the gravity-fed input component, and the exhaust component, which is moderated by a peristaltic pump. The purpose of the system is to provide nutrient- and oxygen-enriched electrolytic solution to the tissue sample while removing metabolite- and waste- enriched solution. This superfusion system is intended to mimic physiological conditions as closely as possible in the compartment that houses the tissue sample.

The catheter opposing the intake port serves as the exhaust port for the metabolite/waste-rich solution after contact with the tissue. This waste fluid is drained from the tissue chamber by a variable rate peristaltic pump (VWR 54856-070). The rate of the peristaltic pump was continuously adjusted to match the flow rate of the gravity-fed intake such that the solution level in the PVC enclosure remained constant.

3.2.3 Preparation of Cortical Tissue Samples

Experiments were performed using a transverse slice preparation of the cerebral cortex of mice; the Animal Care and Facilities Committee at Rutgers University approved this animal protocol. CD-1 mice (Charles River Laboratories) aged from postnatal day 8 (P8) to postnatal day 16 (P16) with a mean age of 10.75 +/- 3.28 days were anesthetized with isoflurane until the absence of a withdrawal reflex from toe pinch. The mice were decapitated and the whole brain dissected in ice cold “slicing” saline solution containing: 7 mM NaCl, 3 mM KCl, 5 mM HEPES, 30 mM D-glucose, and 276.5 mM sucrose; the pH of

this solution was previously adjusted to 7.4. The excised brain was mounted (with cyanoacrylate glue) to an agar block backing with the dorsal side of the brain facing up. Progressive sections of 800 μm thickness were made in the rostral to caudal direction using a vibrating blade microtome (Leica VT 1200). The process of dissection and slicing constitutes a combined hypoxic, ischemic, thermal, and mechanical trauma to the brain tissue (Richerson and Messer, 1995). In order to minimize injury to the tissue as a result of the slicing process, as well as any future injury, the prepared slices were placed in a room temperature "slicing" saline bath saturated with 100% O_2 until utilized for experimentation.

3.2.4 Impedance Analysis

The signal analyzer used in this experimental setup, which has been previously described by Prodan et al. (2004), provides a sinusoidal voltage at its signal output. The voltage at channels 1 and 2 are digitized, the ratio of these two voltages as function of frequency was calculated and the real and imaginary parts of this ratio recorded. The bottom electrode is held at a relative ground potential through the negative input of the amplifier A_2. The output voltage from the signal analyzer was applied to the upper electrode, through resistor R_1. As a result, the current, I, that flows through the sample produces a voltage V_1, which is calculated by Ohm's Law and equates to the product of the current (I) and the impedance (Z) of the sample. The voltage V_2 is also calculated by Ohm's Law and equates to minus the product of the current (I) and resistance (R_2). Therefore, the transfer function, T, is related to the tissue impedance by: $T=R_2/Z$. R_2 is held at a constant 100Ω in these experiments. If the impedance is not contaminated by the polarization effect, then the complex dielectric function $\varepsilon^* = \varepsilon + \sigma/j\omega$ of the sample can be calculated from:

$$Re\{|Z|\} = \frac{d\sigma}{\sigma^2 A + \omega^2 \varepsilon_0^2 \varepsilon^2 A} \tag{3.1}$$

$$Im\{|Z|\} = \frac{\omega d \varepsilon_0 \varepsilon}{\sigma^2 A + \omega^2 \varepsilon_0^2 \varepsilon^2 A} \tag{3.2}$$

3.3 Results of Testing

As aforementioned, superfusion of the tissue is very important and should be done continuously to ensure it is not deteriorating. However this process generates air bubbles, which introduced error during the measurements.

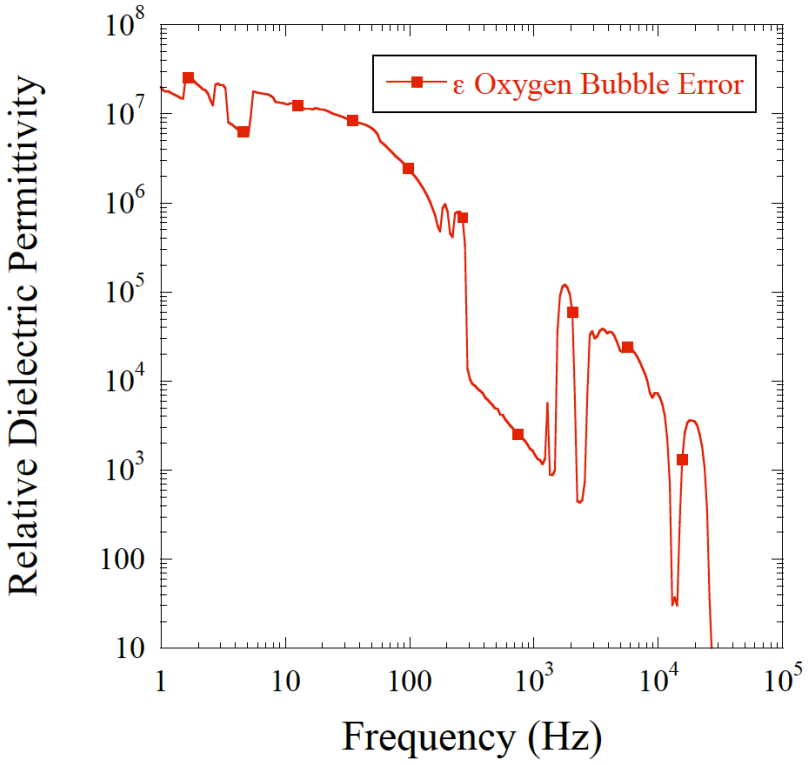

Figure 3.3 The effect of electrolyte oxygenation in the 60 mL reservoir is apparent in that the oxygen bubbles create large amounts of noise in the spectra. This error is avoided by oxygenating the solution prior to placement in the 60 mL syringe.

Figure 3.3 represents avoidable noise attributed to bubbling the 100% oxygen directly into the 60 mL reservoir. Each sharp deviation represents a bubble between the electrodes, which clearly induces error in the measurements. Therefore, in order to avoid this error, the

solution was oxygenated in a 100 mL beaker and incrementally added to the 60 mL syringe at the approximate rate of consumption (6 mL/min) in order to avoid deoxygenating of the solution. This procedure produced dielectric permittivity spectra with minimal noise, as depicted in Figure 3.6.

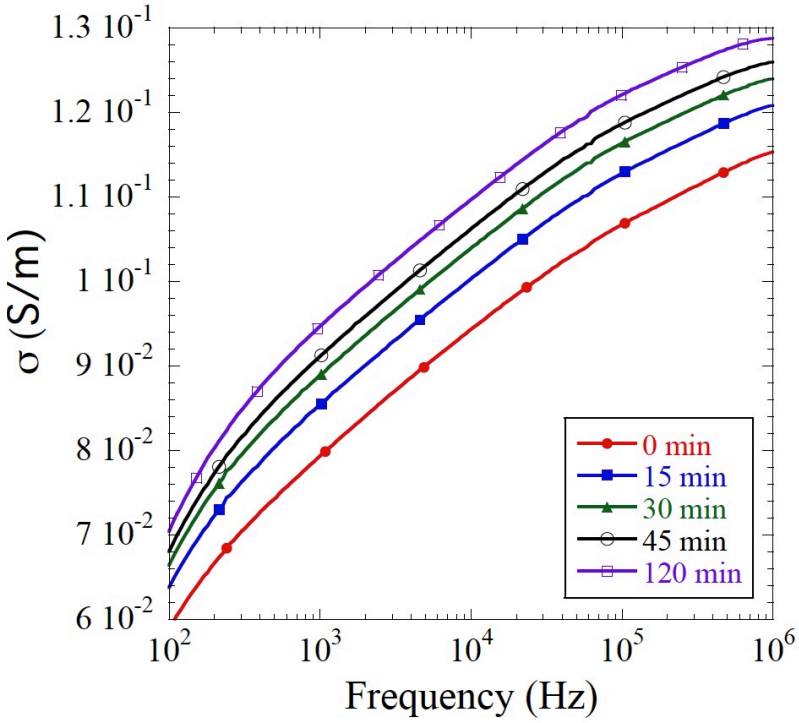

Figure 3.4 Time series of conductivity versus frequency for a slice of tissue without any superfusion. As time increases so does the conductivity of the sample.

If tissue is not superfused and oxygenated, it deteriorates with the passing of time (Hajos and Mody, 2009). This deterioration is seen in the dielectric measurements as an increase in conductivity due to ions released in the solution. Figure 3.4 represents the conductivity versus frequency for a slice of tissue prepared and measured as described earlier but without any superfusion. Here, the tissue is kept in between the electrodes for 2h in the same solution; it can be observed that the conductivity increases in time. Figure 3.5 represents the conductivity data from Figure 3.4 plotted at a single frequency of 1000Hz.

Within 15 minutes, there is a large increase in the conductivity of the solution and tissue of 0.6 mS/m. As time increases, so does conductivity and after 2 hours there is an increase of 1.5 mS/m.

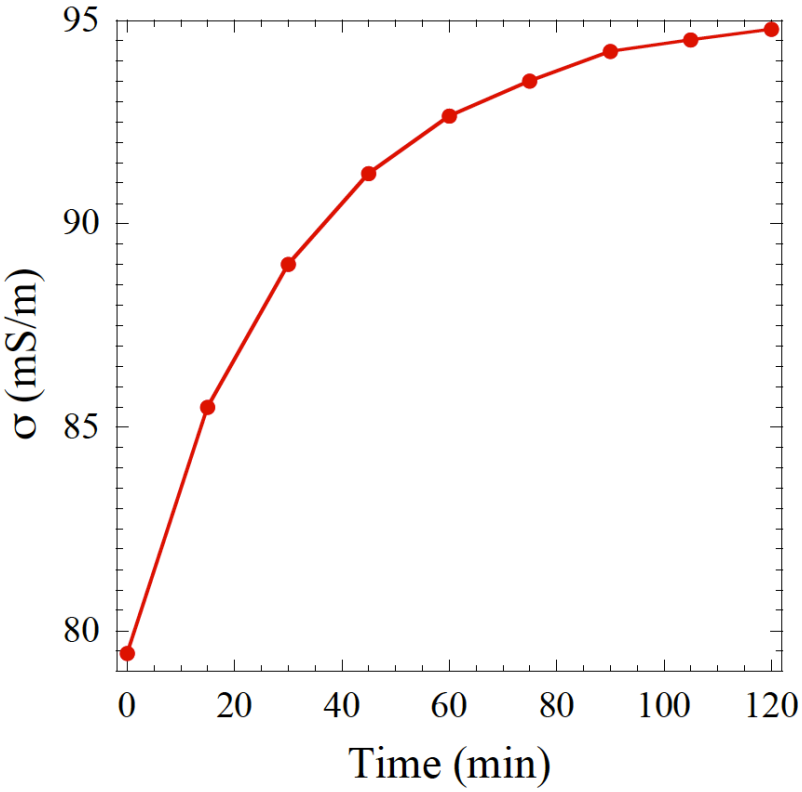

Figure 3.5 Conductivities from Figure 3.4 plotted at a single frequency of 1000Hz. One can see the dramatic change in conductivity as the time increases.

Figure 3.6 represents measurements of tissue in solution prepared as described above. The blue curve represents measurements with the superfusion while for the red one the superfusion system was inactivated. For the same slice of tissue, the measurements were done with perfusion on and off and the data recorded. The error bars for both curves are for n=4 experiments.

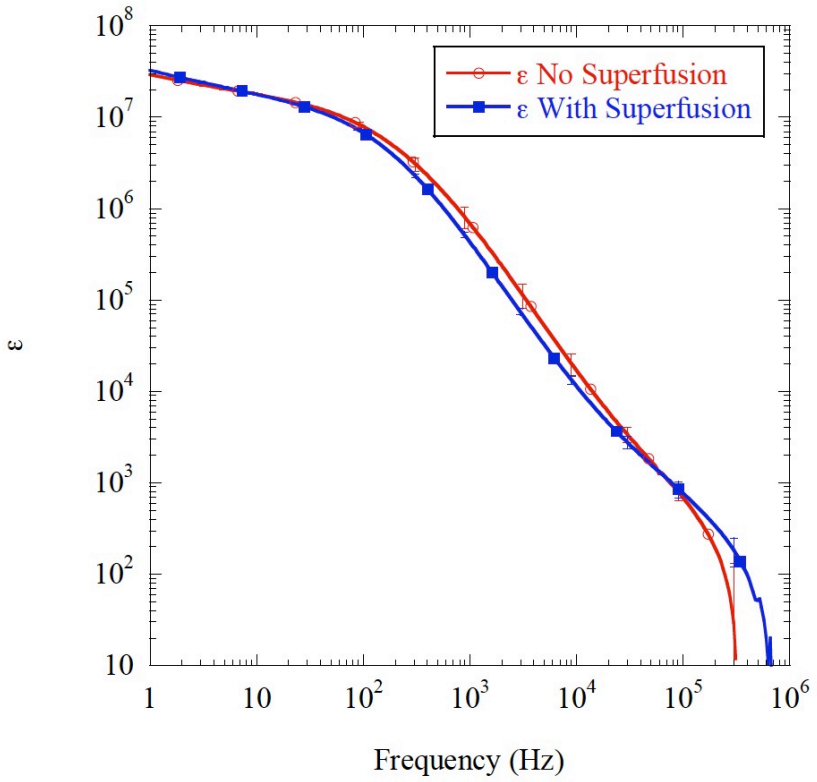

Figure 3.6 The relative dielectric permittivity spectrums with and without the superfusion system engaged. The significant overlap of the spectra in several different frequency ranges suggests that the engagement of the superfusion system has no negative effects on the ability to probe the dielectric properties of the tissue.

When the relative dielectric permittivity spectrum with superfusion time series is compared to the spectrum without superfusion, significant overlap is found in several frequency regions of the spectrum. Therefore, we conclude that the superfusion system has no adverse effects on our ability to probe the dielectric properties of the tissue. In fact, qualitatively analyzing the standard deviation error bars suggests that the superfusion system may result in an increase in trail precision and repeatability because the standard deviations are significantly reduced for the superfusion data. The small differences may be due to the fact that the conductivity for no superfusion already started to increase by a little which, as expected, pushes the curve toward right in the alpha dispersion.

3.4 Discussion of Results and Conclusion

This chapter presents a superfusion method to be used during dielectric spectroscopy measurements to maintain the viability of *in vitro* tissue slices. To keep the tissue healthy during recordings, it has to be continuously oxygenated and provided key nutrients. This process should not interfere with the experiment by creating noise. We investigated here several possibilities of oxygenation and found that it should be done in the syringe while the flow is kept running. It was concluded that a slow flow does not interfere with the measurement by creating errors. It was found that a larger flow compromises the mechanical stability of tissue in the chamber and should not be used. If the tissue is not superfused, the conductivity of the solution changes dramatically in time, as shown above. This implies that ions are released in the solution, which should dramatically change the dielectric response, covering the real response of the tissue.

Another problem with the change in the ion concentration is the electrode polarization error. It is already determined (Bordi *et al.*, 2001; Prodan and Bot, 2009) that even a small increase in the ion concentration increases dramatically the polarization error. The superfusion system presented here does not remove the polarization error but it keeps it constantly in time since the ions are continuously washed away. This way, the response of the tissue only to different insults can be calculated. The superfusion system could potentially be used as a way to deliver pharmaceutical compounds to the tissue. Therefore, the tissue is continuously bathed in a known concentration of the given compound. This set up is similar to the one used in pharmaceutical testing at the cellular level by patch clamping.

Dielectric spectroscopy is a noninvasive technique to monitor in a rapid matter the electric properties of cells and tissues. While patch clamping remains the “golden standard”

to monitor such activities, it is slow and can be done only one cell at the time. Thus, if the dielectric response of a tissue slice is understood, one can imagine real time recording from the whole slice. Dielectric properties of cells have been studied and modeled for a long time. It is known that the alpha response, the low frequency dispersion curve, is strongly influenced by the membrane potential and by the activity on the ion distribution on the outer part of the membrane (Bot and Prodan, 2009). The beta response influenced by the properties of the membrane and of the cytoplasm while gamma is dominated by the individual molecules. To obtain such information, the real behavior of the dielectric response of the tissue has to be recorded. This implies that the tissue has to be kept healthy even during long time measurements and this can be done by bathing (Haas *et al.*, 1979). Also the polarization errors should be removed by existing methods (Bordi *et al.*, 2001; Kaatze and Feldman, 2006; Prodan and Bot, 2009). To conclude, this chapter presents a superfusion method that could be used with dielectric spectroscopy set up. It allows the bathing in a continuously fresh solution of nutrients and oxygen, which is known to keep the tissue steady. This allows measurements in the range of several hours on a healthy tissue.

CHAPTER 4

CORRELATING EXTRACELLULAR FLUID CONDUCTIVITY CHANGE WITH INSULT SEVERITY USING DIELECTRIC SPECTROSCOPY

4.1 Background Information

The maintenance of transmembrane ionic gradients is fundamental for a stable cellular membrane potential (Kettenmann *et al.*, 1983; Hodgkin and Keynes, 1955) and for the viability of neurons (Husted and Reed, 1977). The cellular death mechanisms of necrosis and apoptosis are often preceded by a net efflux of ions from cells (Bortner *et al.*, 1997; Warny and Kelly, 1998; Remillard and Yuan, 2004). Ionic homeostasis dysfunction may result from, or be exacerbated by, a number of pathological conditions, including cocaine abuse (Du *et al.*, 2006), hypoxia (Murai *et al.*, 1997; Müller and Somjen, 2000), and traumatic head injury (Takahashi *et al.*, 1981; Santhakumar *et al.*, 2003).

Dielectric spectroscopy (DS), a technique that characterizes a medium's impedance as a function of frequency, has been used to investigate a variety of cellular and tissue properties, such as membrane potential (Bot and Prodan, 2009), membrane structure and properties (Gheorghiu and Gersing, 2002; Cametti *et al.*, 2011; Ron *et al.*, 2008), glucose concentration in tissue (Caduff *et al.*, 2006), and to distinguish between the different cellular death mechanisms (Lee *et al.*, 2009). DS has also been used to investigate pathology-induced biophysical changes in tissue (Gersing, 1998; Egot-Lemaire *et al.*, 2009; O'Rourke *et al.*, 2007; Schaefer *et al.*, 2002). While DS has been used to determine the conductivity of brain tissue (Schmid *et al.*, 2003) and the dielectric properties of aqueous ionic solutions (Chen and Hefter, 2003; Cametti *et al.*, 2011), no previous investigations have assessed whether a correlation exists between the conductivity of the extracellular fluid surrounding a

brain slice and the health of brain tissue.

In this chapter, a bio-sensing method to assess, in a relatively noninvasive way, the health of a tissue by measuring the conductivity of electrolytic solutions in which cortical brain tissue slices from CD-1 mice were bathed is described. Several insults such as hyperkalemia, hypokalemia, and oxygen-glucose depravation were imparted on the tissue, using tissue from two age groups of mice: weanling and neonatal. It appears that these treatments lead to significant changes in conductivity of the bathing solution surrounding the brains slices, suggesting that dielectric spectroscopy may be used to measure the viability of brain tissue.

4.2 Methodology

4.2.1 Experimental Solutions

Solutions, with varying concentrations of several key constituents (as detailed in Table 1), served as the bathing media for the cortical tissue slices. These solutions were intended to mimic pathological conditions such as hypokalemia, hyperkalemia, and oxygen-glucose deprivation. They were buffered with 5 mM HEPES, and their pH values were adjusted to 7.4 using 1N NaOH or 1M HCl. Osmolarity was adjusted to a measured value of 310 mOsm (using a Wescor Vapro 5600 vapor pressure osmometer) by adding an appropriate concentration of sucrose. All solutions were saturated via an air stone with 100% oxygen, except for the oxygen-glucose deprivation (OGD) solution, which was saturated with 100% nitrogen.

To better observe ion flux, the ionic concentrations of the solutions were maintained low, thus minimizing the initial conductivity of the solution. Thus, we utilized a total of 10

mM of monovalent cations (K^+ and Na^+) and 10 mM of a monovalent anion (Cl^-). To vary the extracellular K^+ concentrations, an increase in K^+ concentration was matched by an equimolar decrease in Na^+ concentration. While the concentration of sodium in the cerebrospinal fluid (CSF) is approximately 147 mM (Morrison, 2008), the majority of transmembrane sodium channels are usually closed at the resting membrane potential, so this low extracellular Na^+ level has little influence on membrane potential (van Mil *et al.*, 2003) and, therefore, should not damage the neural tissue.

Table 4.1 Ion Compositions of Experimental Solutions

Solution	**[KCl]** (mM)	**[NaCl]** (mM)	**[D-Glucose]** (mM)
Control	3	7	15
Severe Hypokalemia	0	10	15
Moderate Hypokalemia	1	9	15
Hyperkalemia	10	0	15
Oxygen-Glucose Deprivation	3	7	15

4.2.2 Preparation of Cortical Tissue Samples

Experiments were performed using a slice preparation of the cerebral cortex of CD-1 mice; the Animal Care and Facilities Committee at Rutgers approved this protocol, which is also in accordance with EU directive 86/609/EEC. CD-1 mice were either obtained directly from Charles River Laboratory (Wilmington, MA) or bred from Charles River Laboratory stock. Two experimental age ranges were used: "neonatal" mice ranged from postnatal day 0 (P0) to postnatal day 2 (P2) and "weanling" mice ranged from postnatal day 14 (P14) to postnatal day 16 (P16). Mice were anesthetized with isoflurane until the absence of a withdrawal reflex from toe pinch. The mice were decapitated and the whole brain dissected in ice-cold slicing solution containing: 7 mM NaCl, 3 mM KCl, 5 mM HEPES, and 15 mM D-glucose.

The pH was adjusted to 7.4 with 1N NaOH or 1M HCl and the osmolarity was adjusted to 310 mOsm with sucrose. The excised brain was mounted (with cyanoacrylate glue) to an agar block backing with the dorsal side of the brain facing up. Progressive sections in the coronal plane were made in the rostral-to-caudal direction using a vibrating blade microtome (Leica VT 1200). The brain slices were then incubated for a period of at least 15 minutes in room temperature saline saturated with 100% O_2.

4.2.3 Exposure of Brain Tissue to Experimental Solutions

In order to supply brain tissue slices with the appropriate gaseous mixture, incubation chambers were constructed from 1.5 mL microcentrifuge tubes. Attempts to oxygenate the tissue via direct flow of gaseous oxygen into the bathing solution resulted in the formation of large bubbles that caused the mechanical disintegration of the tissue slices. Therefore an interface between the oxygen and the bathing solution was required (Figure 4.1). A composite of poly(dimethylsiloxane) (PDMS) (Silgard 184; Dow Corning, Midland MI USA) and 1 mm soda glass beads was utilized as this interface. PDMS was chosen as the membrane material because of its excellent oxygen permeability (Hitoshi *et al.*, 2005) and the reinforcing beads were utilized to support the gas conduit and the PDMS membrane. Gas flow was supplied to the solution through a 30 G subcutaneous syringe, which was inserted through the side of the microcentrifuge tube such that the tip of the syringe came to rest immediately below the surface of the PDMS. To further increase the oxygen saturation of the bathing solution, oxygen was also supplied via a small gauge syringe integrated in the cap of the microcentrifuge tube into the airspace just above the bathing solution. A small hole in the cap of the tube enabled the equalization of pressure.

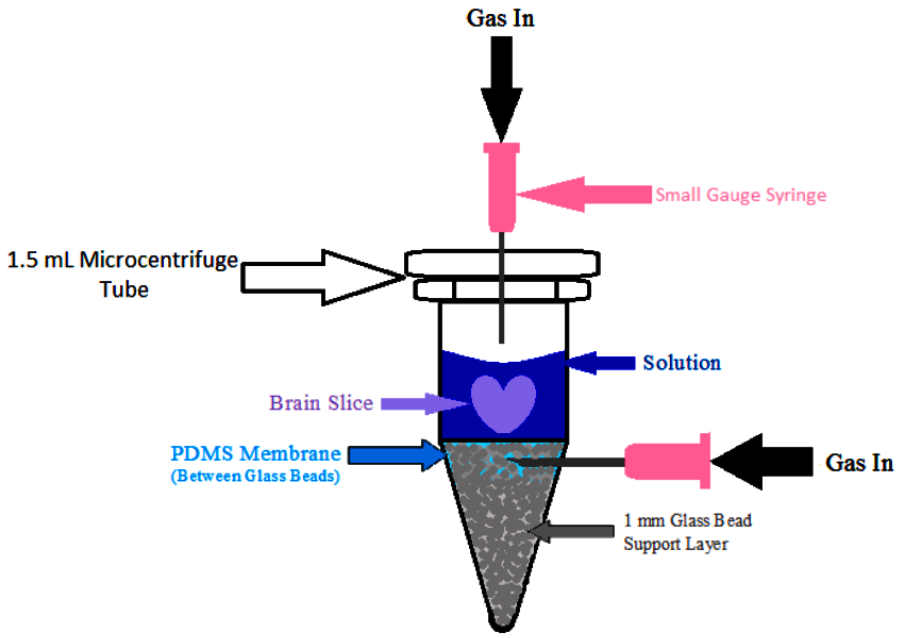

Figure 4.1 A custom incubation chamber consisting of a 1.5 mL microcentrifuge tube was used to bathe 600 µm thick cortical brain tissue slices in experimental solutions that mimic various pathological conditions. A novel composite material, consisting of 1.0 mm-diameter soda glass beads embedded in a polydimethylsiloxane matrix, allowed for adequate supply of experimentally-dictated gas (oxygen or nitrogen) to the tissue slice without causing mechanical trauma to the tissue slice due to its interaction with large gas bubbles.

All experiments were performed at room temperature (23° C). Prior to the exposure of the brain slices to each experimental solution they were washed to rid them of any remnant of the slicing solution. Each slice was transferred to a microcentrifuge tube followed by the removal of all solution via micropipette. The slice was then immediately washed with 0.2 mL of the experimental solution, which was then removed after 60 seconds. This step was subsequently repeated. Subsequently, the tissue was transferred to one of the previously described modified incubation tubes. Pure oxygen, or nitrogen in the case of oxygen-glucose deprivation (OGD), was supplied at this point. 325 µL of the desired

experimental solution (control, hyperkalemia, OGD, etc.) was transferred into the modified incubation tube. Concurrently, a 325 μL sample of the experimental solution was collected without exposure to tissue and preserved in order to act as a basis for conductivity change comparison. The tissue was bathed in the experimental solution for 20 minutes, at which point it was removed from the tissue. The extracellular bathing solution was removed for later analysis while the tissue sample was discarded at this point. Consequently, only the conductivity of the bathing solution was analyzed. The exposed solution and non-exposed solutions were stored at -20° C until analysis by DS occurred.

4.2.4 Conductivity Measurements and Analysis

DS, which has previously been shown to successfully probe the conductivity of polyelectrolyte solutions(Bordi *et al.*, 2004), was utilized to measure the complex conductivity of each solution sample. The electrode system has been previously described (Dobiszewski *et al.*, 2011) and shown to successfully measure conductivity. Briefly, the electrode system consisted of two 14 karat gold electrodes held parallel to one another at a precise distance apart. Prior to measurement of each solution, the distance between the electrodes was calibrated using Milli-Q water.

The impedance analyzer (Solartron 1260; Solartron Analytical Hampshire, UK) and electrical circuit (custom) have been previously described by (Prodan *et al.*, 2004) and (Bot and Prodan, 2009). The complex conductivity function $\sigma=\sigma'+i\omega\varepsilon_0\varepsilon$ of the sample can be calculated from the expression for the impedance (Z):

$$Z = \frac{d\sigma + i\omega d\varepsilon\varepsilon_0}{\sigma^2 A + \omega^2\varepsilon^2\varepsilon_0^2 A} \tag{4.1}$$

The obtained conductivity spectra were calculated from the experimental (impedance) data by a custom Matlab program utilizing the relationship:

$$\sigma(\omega) = \mathbf{Re}\left\{\left(\frac{1}{Z(\omega)}\right)\left(\frac{d}{A\,R}\right)\right\} \tag{4.2}$$

Dielectric spectroscopy measurements were made on each solution from 100 Hz to 1 MHz at a probing voltage of 50 mV. Here we present our analysis of conductivity at 100 Hz, which is within the range used by others (Akhtari *et al.*, 2006). The conductivity of each solution was calculated via a custom Matlab program. The change in conductivity was defined as the difference between two solutions: a test solution exposed to the tissue slice and a control solution that was not.

4.2.5 Statistical Analysis

Statistical analyses were performed using SigmaPlot v. 11.0 (Systat Software, San Jose, CA). A two-way ANOVA, with experimental condition (control, severe and moderate hypokalemia, hyperkalemia, oxygen-glucose deprivation) and age (neonate vs. weanling) as factors, was performed. Where significant main effects of age, experimental condition, or an interaction between the two were found, pair-wise *post hoc* tests (Holm-Sidak method) were performed for comparison. If a significant interaction was found, main effects were discarded. For all tests, a p value of < 0.05 was considered significant. Reported values are expresses as mean ± SEM.

4.3 Results of Conductivity Studies

In order to provide proof that our measurement system was capable of measuring the strong electrolytes likely to be encountered in the extracellular solutions of the brain, we first

assessed the molar conductivity of a prototypical strong electrolyte (KCl) with respect to molar concentration; the results are presented in Figure 4.2. Notice that the result presented in this figure follows the power law relationship described by Kohlrasuch's Law (Coury, 1999). Therefore, it is deduced that the system can accurately measure the conductivity of strong electrolytes.

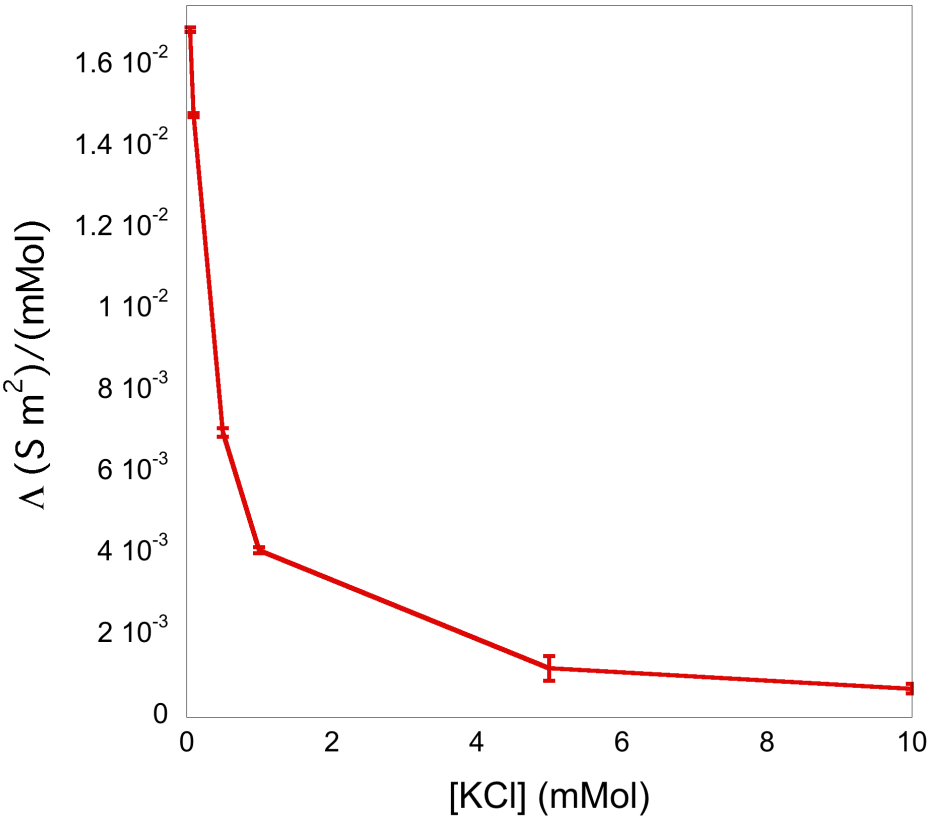

Figure 4.2 The molar conductivity of a strong electrolyte solution (KCl) with respect to molar concentration is presented as the solid line. Kohlrausch's law theoretically defines the relationship between molar conductivity (Λ) and molar concentration as a power law regression for all strong electrolytes.

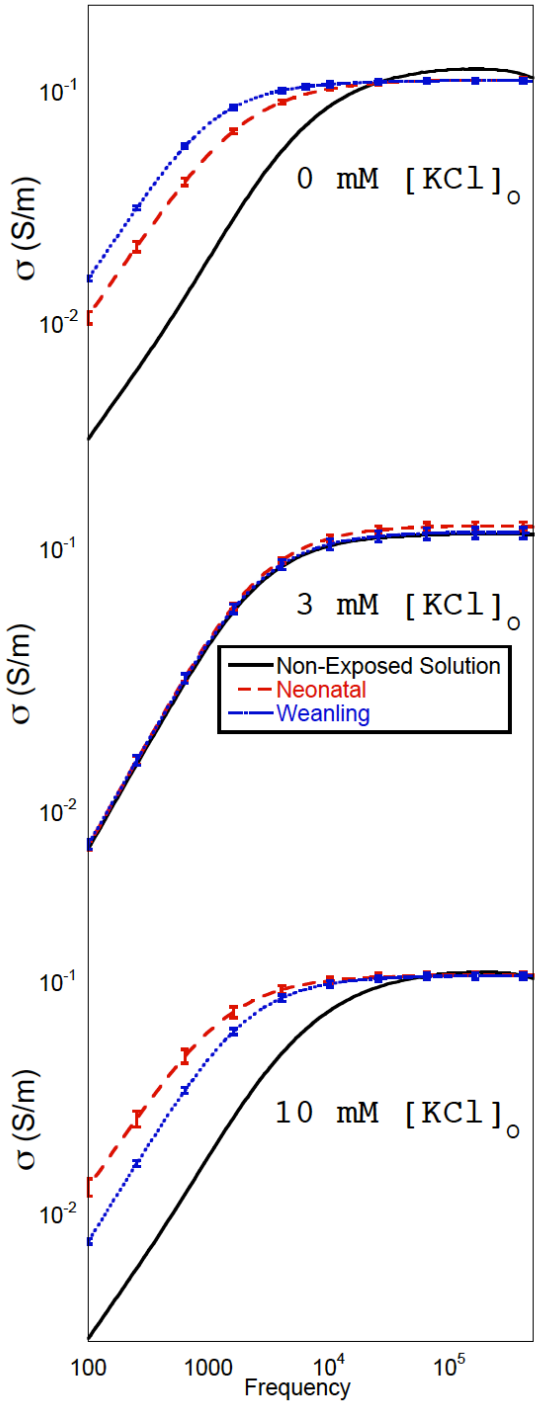

Figure 4.3 Conductivity with respect to frequency from 100 Hz to 1 MHz for three different extracellular potassium concentrations (severe hypokalemia, control, and hyperkalemia). In all the graphs, the solid line (——) represents the solution that never came in contact with the tissue slice, the dotted line (.....) represents the conductivity of the solution after exposure to the tissue slices from weanling-aged (P15-P17) mice, and the dashed line (– –) represents the conductivity of the solution after exposure to tissue slices from neonatal-aged (P0-P2) mice.

The focus of this study was the analysis of the change in conductivity of extracellular solutions subsequent to bath exposure with live cortical tissue. Furthermore, because the neural response to pathologic conditions can change as a function of age, two distinct age ranges were tested: neonatal and weanling.

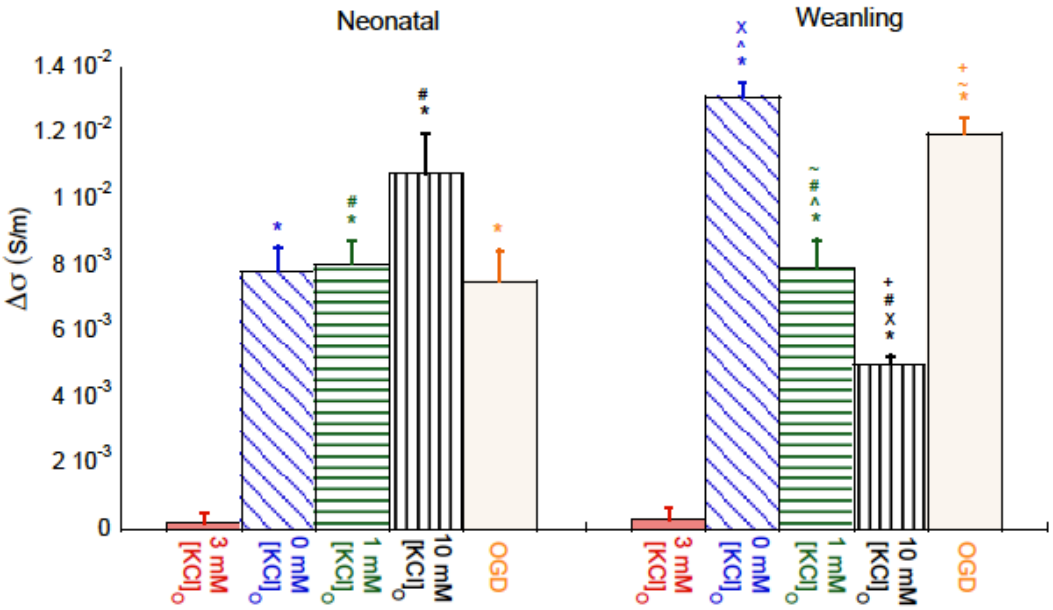

Figure 4.4 Changes in conductivity at 100 Hz of the various experimental solutions (control, severe and moderate hypokalemia, hyperkalemia, and oxygen-glucose deprivation) in which cortical tissue slices were bathed. Significant changes (denoted '*'; $p>0.05$, n= 6-15) in conductivity with respect to the control condition (3 mM $[KCl]_O$) are seen in all experimental conditions over both age ranges tested (weanling and neonate). Additionally, significant changes ($p>0.05$) between different pairings of pathological conditions are denoted by '^', 'X', '#', '~', and '+'.

Figure 4.3 represents the conductivity versus frequency corresponding to "severe hypokalemia" (0 mM $[KCl]_O$; top), control (3 mM $[KCl]_O$; middle), and "hyperkalemia" (10 mM $[KCl]_O$; bottom). As one can see, for "severe hypokalemia", the spectrum for the weanling was greater than the spectrum for the neonatal at low frequencies. However, at higher frequencies (above approximately 10 kHz), the spectra for both ages converged and eventually overlapped. For the "hyperkalemia" condition, this trend was reversed; the

spectrum corresponding to the neonates was greater than that of the weanlings at low frequencies. At higher frequencies, the spectra for both age ranges converged and eventually overlapped. The middle graph represents control conditions (3 mM $[KCl]_O$) and was characterized by overlapping spectra for neonates and weanlings at all frequencies.

Figure 4.4 shows the change in extracellular conductivity of the various experimental solutions after exposure to brain slices. In tissue from weanlings, all three experimental extracellular K^+ concentrations produced statistically significant increases in conductivity compared with the control solution (3 mM KCl). The largest change in conductivity was in response to severe (0 mM $[KCl]_O$) hypokalemia. The increase in conductivity, resulting from moderate (1 mM $[KCl]_O$) hypokalemia was less than the increase in severe hypokalemia. Furthermore, the increase in conductivity was lower in response to hyperkalemia (10 mM $[KCl]_O$) compared to moderate and severe hypokalemia. Therefore, in weanlings as the extracellular potassium concentration was varied there were graded increases in conductivity, with severe hypokalemia leading to the greatest change and hyperkalemia leading to the least change. In response to OGD, there was a greater increase in conductivity compared with the control solution in weanlings. This increase was significantly different from those observed after exposure to moderate hypokalemia and hyperkalemia (Figure 4.4).

In the neonates, all experimental conditions produced statistically significant changes when compared to the control solution (3 mM KCl). However, unlike the weanling data, there was no significant difference between exposures to moderate hypokalemia and severe hypokalemia. Furthermore, in neonates the increase in conductivity was significantly greater in hyperkalemic solution compared to moderate hypokalemic solution. This is different from the response observed in weanlings, in which the increase in conductivity was significantly

smaller in hyperkalemic solution compared to moderate and hypokalemic solutions. In response to OGD, there was a greater increase in conductivity than that observed with the control solution. Unlike the weanling data, in which the response to OGD was greater than that to moderate hypokalemia and hyperkalemia, in the neonate, there were no significant differences between the response to OGD and the responses to the three experimental potassium concentrations.

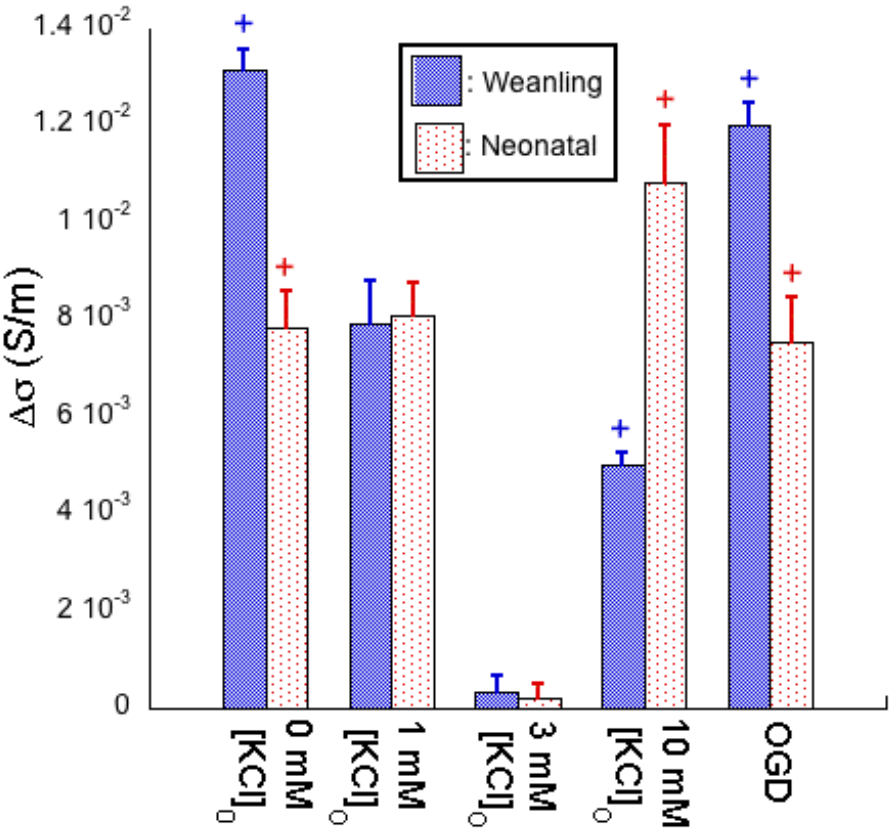

Figure 4.5 Change in conductivity (at 100 Hz) of solution due to exposure to tissue slice as a function of the mouse age. Significance (P>0.05) between age groups within the same experimental condition is denoted by '+' above each bar.

In Figure 4.5, the data corresponding to the change in conductivity was plotted to facilitate the comparison of the changes caused by each experimental solution between the

two age ranges. Both severe hypokalemia and OGD produced significantly greater changes in weanlings compared to neonates. In contrast, the hyperkalemic solution produced a significantly greater increase in conductivity in neonates compared to weanlings.

4.4 Discussion of Conductivity Studies

In this chapter, the extracellular concentration of the potassium ion (K^+) in solutions in which cortical brain slices were bathed was altered (0 mM $[KCl]_O$, 1 mM $[KCl]_O$, 10 mM $[KCl]_O$) with respect to its normal physiological value. Under physiological conditions, the intracellular concentration of K^+ is many times greater than the extracellular cerebrospinal fluid (CSF), which has a K^+ concentration that varies between 2.7 and 3.5 mM (Somjen, 2002). Deviation from this range leads to biophysical changes to the cells that impair neural function. Low extracellular K^+ concentrations lead to hyperpolarization (Kuwabara *et al.*, 2002), increased intracellular Na^+ concentration (Korff *et al.*, 1984), and the induction of apoptosis (D'Mello *et al.*, 1993). Elevation of extracellular K^+ concentration has pathological consequences and is so lethal that a large exogenous dose of K^+ is used for capital punishment (Wong, 2006). Under pathological conditions, such as epilepsy and stroke, the uppermost concentration limit of extracellular K^+ in the brain is approximately 12 mM (Heinemann and Lux, 1977). During instances of head injury, the cortical extracellular potassium concentration can reach as high as 50 mM (Takahashi *et al.*, 1981).

In the current chapter, a graded response to changes in the extracellular K^+ concentration was observed in cortical tissue from weanling mice. Severe hypokalemia led to significantly greater increases in extracellular conductivity compared to moderate hypokalemia or hyperkalemia. In contrast, there was no difference between the response to moderate and severe hypokalemia in neonates. Additionally, the response to hyperkalemia

was significantly greater in neonates compared to weanlings. These results are consistent with the notion that compared to older mice, neonates have a limited ability to regulate the K^+ concentration in the cerebrospinal fluid (Jones and Keep, 1987).

In order for cells in the brain to maintain a constant extracellular concentration of potassium, the input of metabolic energy is essential. While the brain accounts for only a small percentage of total body weight, it accounts for nearly 20% of the body's total oxygen consumption; 70% of which is used to provide energy for the Na^+/K^+ ATPase (Edvinsson and Krause, 2001), an enzyme that helps to maintain ionic concentration gradients across the plasma membranes of cells (Rossier *et al.*, 1987). Accordingly, the dysfunction of the Na^+/K^+ ATPase in brain cells leads to cellular death (Magyar *et al.*, 1994). Deprivation of cellular oxygen and glucose input leads to a reduction in intracellular ATP and an indirect shutdown of the Na^+/K^+ ATPase (Hertz, 2008), potentially resulting in ionic hemostasis dysfunction (Thompson *et al.*, 2006) and necrotic cell death (Miyamoto and Auer, 2000).

Based on this information, it is logical to hypothesize that a large increase in conductivity would occur during OGD. Interestingly, the increase in conductivity following OGD was significantly smaller in neonates compared to weanlings (Figure 4.5). This difference likely corresponds to the observation that neonates possess a greater ability to withstand the OGD compared to older animals (Haddad and Donnelly, 1990). Also of interest, the increases in extracellular conductivity in the severe hypokalemic and OGD groups were similar within each respective age group (Figure 4.4). This observation may be due to the effect that both conditions have on the Na^+/K^+ ATPase. As the concentration of extracellular potassium diminishes, the efficacy of the ATPase is markedly decreased (Heidlage and Jones, 1981). Similarly, as the amount of available ATP decreases during

OGD, inhibition of Na^+/K^+ ATPase activity occurs (de Souza Wyse *et al.*, 2000). Therefore, it is possible that the state of dysfunction and poor cellular health in both cases is similar.

Since these measurements were conducted at low frequencies, it is quite likely that the electrical double layer effect dominates the measurements. The effect of this double layer impedance, which has been described by numerous researchers for decades, varies dramatically with both ionic concentration and frequency. Instead of viewing this double layer as a hindrance to collecting useful information, it was actually used it to the advantage of the researchers. Painstaking measures were taken, such as precisely maintaining the ionic concentrations presented in Table 4.1, to ensure that the initial conductivities of baseline solutions were identical prior to the addition of the tissue. To ensure proper ionic concentrations in our solutions, a conductivity meter and osmometer were both utilized. Furthermore, instead of trying to remove the effect of the double layer impedance, the focus of the researchers was evaluating the conductivity differences from these precise baseline solutions in order to use DS as a sensor. Thus, any variation from the initial conductivity of the solution represents the response of the tissue to the insult.

While the change in extracellular solution conductivity is clearly frequency-dependent, it is likely that the change is also time-dependent. In pathological conditions such as ischemia (OGD), there is a rapid and punctuated rise in extracellular potassium concentration within minutes of the OGD onset (Hansen, 1985). Subsequently, the extracellular potassium concentration plateaus around 50 mM for the remainder of the ischemic insult. Given that our exposure duration was 20 minutes, it is possible that a large flux of potassium ions could have contributed to the extracellular solution conductivity.

4.5 Conclusions

Since both necrotic and apoptotic cellular death mechanisms involve a net efflux of ions from the dying cell, evaluation of the extracellular ion profile may provide useful insight into the health and vitality of neural tissue. While methods such as ion-selective microelectrodes measure changes in the concentration of a single ionic species, they lack the ability to simultaneously assess the contribution of several different ionic species. In this chapter, dielectric spectroscopy, which allows for the measurement of the net change in number of all charged particles in solution (i.e., a solution's conductivity), was utilized. This data has shown that dielectric spectroscopy allows for measurements of extracellular conductivity that are sensitive enough to distinguish between the ionic effluxes from brain slices under conditions that mimic different pathological states. Thus, measuring the conductivity of the extracellular bathing solution of neural tissue may be an alternative method for monitoring the health of a tissue specimen. Furthermore, since we are measuring just the conductivity of extracellular fluid and not the fluid and tissue combination, extrapolation of this technique to a clinical setting is more plausible.

CHAPTER 5

MODULATON OF POTASSIUM HOMEOSTASIS BY μ-OPIOID RECEPTOR ACTIVATION DURING SIMULATED ISCHEMIA

5.1 Background Information

While the mammalian brain constitutes only a small percentage of total body area, it consumes approximately 20% of consumed oxygen (Kety, 1957). When brain tissue is subjected to hypoxic/ischemic insult, a cascade of events, including an increased in glutamate concentration (Kulik *et al.*, 2000; Young *et al.*, 1993) a profound shift in both intra- and extracellular ion concentrations (Haddad and Yao, 2004; Hansen, 1985; Chao and Xia, 2010), and depolarization (Haddad and Donnelly, 1990), soon occurs. The shift in ion concentrations is characterized by a net efflux of potassium coupled with a nearly simultaneous net influx of calcium, chloride and sodium (Hansen, 1985; Haddad and Yao, 2004; Jiang *et al.*, 1992).

During periods of hypoxia/ischemia, intracellular potassium is expelled and accumulates extracellularly in a biphasic manner, characterized by an immediate yet modest increase, followed several minutes later by a rapid and profound increase (Hansen and Nedergaard, 1988). The mechanism of this accumulation is complicated but it is believed that a variety of mechanisms contribute to this accumulation. Regardless of the mechanism of this accumulation, it is well documented that the increase in extracellular potassium concentration is responsible for cellular death (Yu *et al.*, 1999; Remillard and Yuan, 2004; Liu *et al.*, 2003). Accordingly, K^+ channel blockers have been shown to attenuate cell death following ischemic insult (Wei *et al.*, 2003). Furthermore, in animals that display resistance

to anoxic injury, such as the turtle, extracellular potassium accumulation occurs much more gradually and with lower magnitude than in mammalian tissue (Xia *et al.*, 1992). Taken together, these observations suggest that mechanisms that decrease extracellular potassium accumulation may be neuroprotective during periods of hypoxia/ischemia.

Opioids are a class of neuropeptides belonging to the G protein-coupled receptor family (Raynor *et al.*, 1994) that can be characterized into three distinct receptor sub-types: the μ-opioid receptor (MOR), the δ-opioid receptor (DOR), and the κ-opioid receptor (KOR). These receptors are widely distributed throughout the mammalian nervous system (Goodman *et al.*, 1980). Opioids are modulators of ionic homeostasis because of their effect on a variety of different ion channels and currents, including potassium (Ikeda *et al.*, 1995), calcium (Su *et al.*, 1998; Toselli *et al.*, 1997), chloride (Kromer, 1993) and sodium (Witkowski and Szulczyk, 2006). Due to this modulatory effect on different ionic currents and the correlation of ionic homeostasis dysfunction with hypoxic/ischemic insult, several groups have investigated the effect of opioid receptor activation during hypoxia/ischemia.

Evidence suggests that DOR activation during oxygen-glucose deprivation (OGD; simulated ischemia) in the rat cortex attenuates the accumulation of extracellular potassium (Chao *et al.*, 2007b; Chao *et al.*, 2012; Chao and Xia, 2010) through the inhibition of sodium and calcium influx (Chao *et al.*, 2008; Chao *et al.*, 2007a; Chao *et al.*, 2012; Kang *et al.*, 2009), thus protecting neural tissue from injury and death (Zhang *et al.*, 2002). Interestingly, while MOR and DOR share similar modulatory effects on some ion channels (North *et al.*, 1987), MOR activation did not show the same capability to modulate potassium homeostasis dysfunction in the cortex (Chao *et al.*, 2007a). This observation may be due to the fact that the cortex contains a higher density of DOR than other parts of the brain (Xia and Haddad,

1991). Indeed, receptor density may play a pivotal role in potassium homeostasis modulation; in turtles, which display remarkably less potassium homeostasis dysfunction during hypoxia than rats (Xia *et al.*, 1992), the cortical DOR density is significantly higher in turtles compared to rats (Xia and Haddad, 2001). Therefore, it is not unreasonable to hypothesize that MOR activation during OGD and/or hypoxia in a region of high MOR density may have a similar effect as DOR activation in the cortex.

The Pre-Bötzinger Complex (preBötC) is a region of the brainstem that is responsible for respiratory rhythm generation (Smith *et al.*, 1991). It is also a region that contains a high density of MOR (Gray *et al.*, 1999). Accordingly, clinical administration of opioid agonists is related to respiratory depression due to effects on preBötC, as well as other brain regions (Boom *et al.*, 2012). Furthermore, the preBötC is sensitive to hypoxia/ischemia in that it acts as a hypoxic chemoreceptor for respiratory function (Solomon *et al.*, 2000) and is intrinsically sensitive to changing ATP concentration (Lorier *et al.*, 2007). These sensitivities manifest as alternations to eupneic respiratory frequency (Solomon, 2002). Because of this high density of MOR and its innate sensitivity to changing oxygen and ATP concentrations, the preBötC is an ideal brain region to investigate MOR activation on potassium homeostasis during periods of hypoxic and ischemic stress.

5.2 Methodology

5.2.1 Experimental Saline and Drug Preparations

All constituents of the experimental saline solutions were purchased from Fischer Scientific (Waltham, MA), unless otherwise noted. The “normal” saline consisted of artificial cerebrospinal fluid (aCSF) with the following composition (in mM): 118 NaCl, 3 KCl, 25

$NaHCO_3$, 1 NaH_2PO_4, 1 $MgCl_2$ x 6 H_2O, 1.5 $CaCl_2$, 30 D-glucose; the pH was adjusted to 7.4 at 32° C by the addition of a gaseous mixture of carbogen (95% O_2/5% CO_2). The "OGD" saline consisted of aCSF with a similar composition as outlined above but with 30 mM sucrose replacing the 30 mM D-glucose; the pH was adjusted to 7.4 at 32° C by the addition of a gaseous mixture of 95% N_2/5% CO_2.

The potent and selective μ-opioid agonist DAMGO was utilized to investigate MOR activation while the non-selective opioid antagonist naloxone hydrochloride was used to abolish DAMGO's effect at the MOR. Both drugs were purchased from Sigma-Aldrich (St. Louis, MO). Stock solutions of DAMGO (60 μM and 500 μM) and naloxone (10 mM) were produced and then stored in aliquots according to manufacturer suggested conditions until used.

5.2.2 Animals

The CD-1 mice used in all experiments were bred from a group of founders purchased from Charles River Laboratories (Wilmington, MA). Special care was taken to only mate males and females with an uncommon lineage, thereby increasing the genetic variability of the offspring. All experimental protocols were developed such that both the number of animals used and their suffering was minimized. These protocols comply with European Union Directive 86/609/EEC and were approved by the Animal Care and Facilities Committee at Rutgers, the State University of New Jersey. For DAMGO dose-response experiments, nineteen mice from 5 distinct litters and ranging in age from postnatal days 6 to 9 (P6-P9) were utilized. For potassium homeostasis experiments, 26 mice (15 Male, 11 Female) from 11 unique litters and aged postnatal days 7 to 11 (P7-P11) were used.

5.2.3 Medullary Slice Preparation

Experiments were performed using a transverse brainstem slice taken from the medulla of young mice (Ramirez *et al.*, 1996). Mice within the appropriate age range were deeply anesthetized with isoflurane until the absence of withdrawal reflex during toe pinch and rapidly decapitated. The brainstem and a short segment of spinal cord were dissected in ice-cold aCSF as efficiently as possible. During dissection, the temperature of the aCSF bathing the tissue was maintained artificially low by the constant addition of aCSF ice chips. Immediately upon completion of the dissection process, the brainstem and spinal cord preparation was mounted (caudal end up and ventral side out) to an agar block with cyanoacrylate glue. A vibratome (Leica VT 1200; Leica Microsystems, Wetzlar, Germany) was used to cut serial (100 μm) sections in the caudal-to rostral direction until the principle loop of inferior olive was visualized. This anatomical marker corresponded to the appropriate rostro-caudal level at which a 500 micron tissue slice containing the preBötC (Ruangkittisakul *et al.*, 2011) was produced.

The dissection and slicing process imparts a variety of stressors upon the tissue (Richerson and Messer, 1995). Therefore, in order to promote vitality, the slice was incubated for twenty minutes in oxygenated aCSF; the temperature of the reservoir was gradually increased to 32° C from room temperature over the course of the incubation period.

5.2.4 Potassium Selective Microelectrodes

Liquid membrane ion sensitive electrode (ISE) technology was utilized to produce microelectrodes capable of accurately measuring extracellular potassium concentrations. Unfilamented electrode glass (0.86 mm inner diameter) (World Precision Instruments Inc.;

Sarasota, FL) was cleansed in 99.9% methanol (Sigma-Aldrich; St. Louis, MO) and then dried on a hot plate at 100° C. Patch pipettes with tip resistance of approximately 9 MΩ were pulled (Sutter Instrument Company P-97; Novato, CA) and the tips then etched and broken to produce a low resistance (2.02 MΩ mean resistance, n=27) straight tip. The inner surface of the electrode was made hydrophobic by the injection of a small volume (50 µL) of liquid dichlorodimethylsilane (99%) (Sigma-Aldrich; St. Louis, MO) into the electrode; the electrodes were subsequently heated at 100° C for approximately two hours. The electrodes were then allowed to cool to room temperature.

The tips of the microelectrodes were carefully filled by capillary action with Potassium Ionophore I- Cocktail B (Sigma-Aldrich; St. Louis, MO) containing 5% valinomycin. Valinomycin is a natural ionophore that is highly selective for potassium over other ions (Tosteson *et al.*, 1967). Care was taken to ensure that no air bubbles were present in the ionophore column and when an adequate volume of ionophore occupied the tip, the electrode was backfilled with 500 mM KCl solution using a microfill pipette. Again, care was taken to ensure a "clean" junction, i.e. no air bubbles or other obstructions, between the ionophore column and the backfill solution. Because the response time of the electrode is dependent on the length of the ionophore column, effort was made to consistently produce columns of similar length. In instances where the column length was too great, gentle pressure was applied to the end of the electrode, thus causing the ionophore to gradually escape the tip. Pressure was applied until the ionophore column length was approximately 100-200 µm.

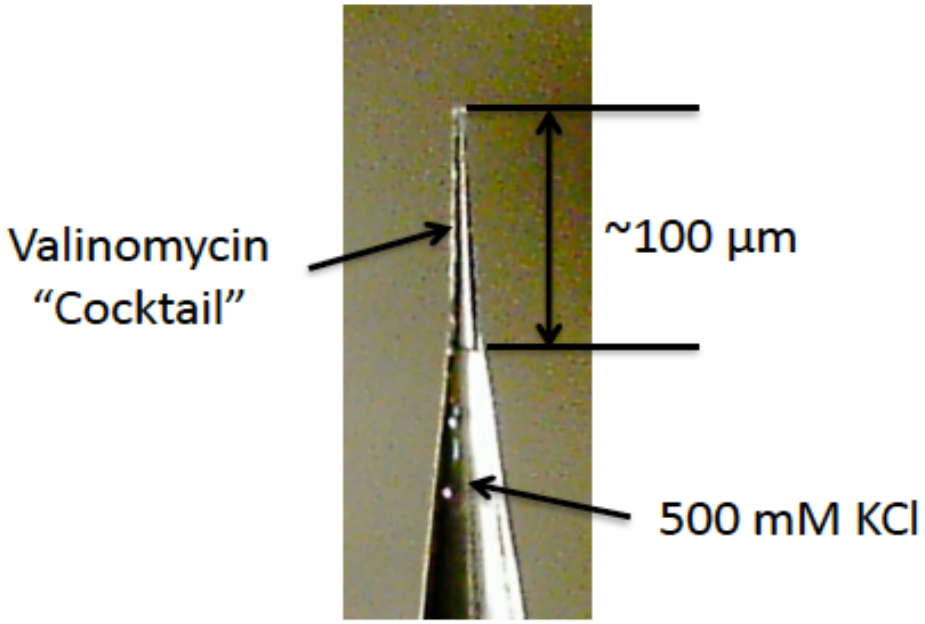

Figure 5.1 Microelectrodes produced from unfilamented capillary glass with a tip resistance of approximately 2 MΩ. The tips of these microelectrodes were filled with a 100-200 µm column of valinomycin "cocktail". The rest of the microelectrode was filled with 500 mM KCl solution. These microelectrodes displayed predictable responses to changing potassium concentrations.

Reference electrodes were produced from filamented electrode glass (0.86 mm inner diameter)(World Precision Instruments Inc.; Sarasota, FL) by pulling electrodes with a low resistance (5-7 MΩ) tip and filling with 3 M KCl solution. A reference electrode was paired with a potassium sensitive microelectrode and the pair was calibrated at room temperature by detecting the voltage response generated by a decade (3 to 30 mM) change in extracellular potassium concentration. This value was then adjusted to account for the fact that experiments would be conducted at 32° C. After temperature adjustment, the average slope per log 10 unit increase in potassium concentration was 55.32 +/ 3.64 mV (n=26). After calibration, the electrodes were stored suspended with tips immersed in distilled water until use.

5.2.5 Electrophysiology Experiments

After the 20 incubation perioid following slicing, the 500 μm slice containing the preBötC on the caudal surface was transferred to the superfusion chamber (RC-29, Warner Instruments; Hamden, CT) and prepared for electrophysiology recordings. To ensure adequate gas exchange, the slice was positioned and supported such that aCSF from the bath reservoir could freely flow both above and below the slice at a flow rate of approximately 10 mL/min; the volume of aCSF in the superfusion chamber at any given point was approximately 2.5 mL. The temperature of the bath solution was continuously monitored and maintained through a feedback loop at 32° C. A Syringe Warmer Power Controller (SW-707) and Syringe Heaters (SW-60) were used to heat aCSF in the bathing reservoirs. A Temperature Controller (TC-344B), platform heater (PM-6D), and inline heater (SH-27B) were used to heat the aCSF both while en route to and while in the superfusion chamber. All heaters and control units were manufactured by Warner Instruments (Hamden, CT).

5.2.5.1 DAMGO Dose-Response Experiments. Bursts of rhythmic extracellular neuronal population activity were recorded by placing a saline-filled pipette on the caudal in the region of the preBötC. The extracellular signal was amplified using a 100-fold gain differential preamplifier (JFIE 1626; James Franck Institute Electronics Laboratory, University of Chicago, IL) in series with a variable gain amplifier (Model 410; Brownlee Precision Instruments, Santa Clara, CA). The raw analog signal was then band-pass filtered (100 Hz to 1 kHz), rectified and integrated with analog circuitry using a time constant of 50 ms (JFIE 1620A Dual Channel Integrator; James Franck Institute Electronics Laboratory, University of Chicago), digitized (Digidata 1440A; Molecular Devices, Sunnyvale, CA), and stored to hard disk for later analysis.

In order to stimulate rhythmic population bursting in the preBötC, the extracellular concentration of potassium was increased to 8 mM (Tryba *et al.*, 2003). After electrode placement on the caudal surface of the slice in the location of preBötC and observation of rhythmic bursting activity, experimental recording was initiated and the rhythm was allowed to stabilize for 30 minutes. After this stabilization period, the slice was exposed to varying DAMGO concentration (1, 50, 150, 250 nM, n=3 each) by changing the superfusate bath reservoir to one containing the prescribed concentration of DAMGO; in a subset of experiments (n=2), no DAMGO was added after the stabilization period (control). After 30 minutes of bath exposure to DAMGO, the superfusate bath reservoir was switched to one containing DAMGO-free aCSF. In order to stimulate complete removal of the drug, the tissue slice was washed with 100 mL of fresh aCSF containing no DAMGO.

To analyze the effect and dose-response relationship of the DAMGO application, the rectified and integrated voltage signal, which shows a positive deflection corresponding to extracellular population bursts (Figure 5.2), was digitally filtered with a 2^{nd} order Butterworth low pass filter (1.5 Hz cut-off frequency) and then inputted into a custom MATLAB program for further analysis. The burst frequency was calculated based on the occurrence of all fictive burst regardless of waveform shape. A sequence of mean burst frequency values was calculated by averaging data from 120-second periods throughout the experiment duration. The burst frequencies during DAMGO application was normalized by dividing each 120-second period during DAMGO application by the 120-second period immediately prior to DAMGO application. The normalized burst frequency for the 120-second period immediately subsequent to the removal of DAMGO and initiation of wash was utilized from each experiment to produce a dose-response curve.

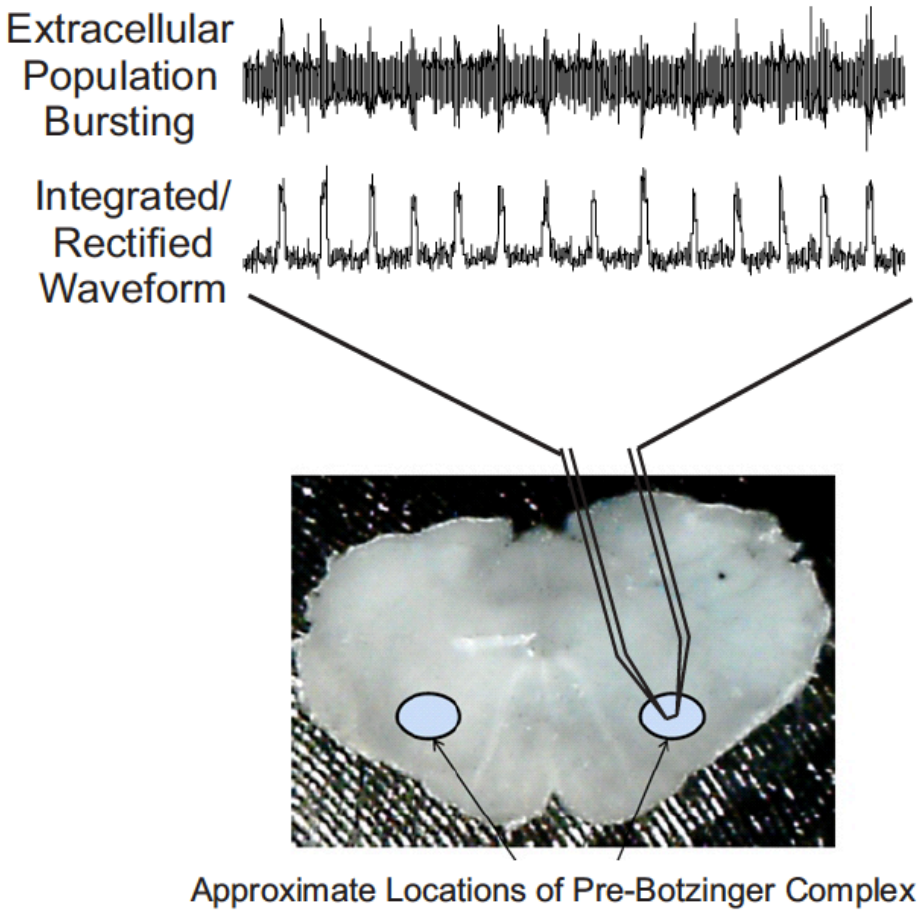

Figure 5.2 Extracellular population bursting activity was recorded using suction electrodes in the area of the Pre-Bötzinger Complex. Each burst in the raw extracellular signal (top) corresponds to a positive deflection in the integrated and rectified waveform.

5.2.5.2 Potassium Measurements During Hypoxia and OGD. Measurements of extracellular potassium concentration were made using the previously described potassium selective microelectrodes and an Axon Multiclamp 700-B amplifier (Molecular Devices; Sunnyvale, CA) in current clamp mode coupled to a Digidata 1440A digitizer (Molecular Devices; Sunnyvale, CA). The spatial orientation of the potassium selective microelectrode was controlled and precisely manipulated by a Burleigh PCS-6000 micromanipulator (Thorlabs; Newton, NJ).

In order to confirm the location of the preBötC, the extracellular concentration of potassium in the superfusate was raised to 8 mM (Tryba *et al.*, 2003) and rhythmic population bursting was observed using the suction electrode method already previously described. After five minutes of observing rhythmic bursting activity, the potassium concentration in the superfusate bath was lowered to 3 mM and the tissue was allowed to acclimate at this new potassium concentration for 15 minutes. As a result of the lower extracellular potassium concentration, rhythmic bursting activity ceased but extracellular tonic activity was still observable. After this 15-minute acclimation period, a potassium selective microelectrode was carefully immersed in tissue in a region of the slice away from the preBötC and allowed to equilibrate in tissue for a 20-minute period. The electrode was then moved to the preBötC and again immersed to a depth of 100 microns. Placement in preBötC was confirmed by immersing the potassium selective microelectrode immediately adjacent to the electrode that had previously been used to record population burst activity.

The experimental procedure underlying the measurement of potassium concentrations during OGD and the effect of DAMGO application during OGD called for several distinct periods during experimentation. After immersion of the electrode in the preBötC, baseline potassium levels and tonic activity levels were recorded for 30 minutes before experimental manipulation of oxygen and/or glucose; this period was referred to as the "baseline" period. In order to compare the accumulation of extracellular potassium between hypoxia and OGD, hypoxia only (n=4) or OGD (n=6) was initiated for a 30-minute period by switching the superfusate to one containing normal aCSF but saturated with 95% N_2/5% CO_2 (hypoxia only) or to one containing "OGD acSF" containing 0 mM D-glucose and saturated with 95% N_2/5% CO_2 (OGD). These OGD experiments would also serve as a control group for the

later evaluation of the effect of MOR activation by DAMGO during OGD. This period of varying oxygen and/or glucose concentrations was referred to as the "manipulation" period. After this "manipulation" perioid, the superfusate was switched to one containing "normal" aCSF saturated with 95% O_2/5 % CO_2, thus entering the "recovery" period. Potassium measurements and extracellular population activity recordings were maintained throughout all periods.

In order to assess the effect of MOR activation by DAMGO during OGD, either 60 (n=6) or 250 nM (n=6) of DAMGO was bath-applied to the slice 10 minutes prior to the initiation of OGD (20 minutes into the "baseline" period). The former concentration represents the EC_{50} for DAMGO-induced depression of respiratory rhythm bursting, while the latter represents a concentration that completely abolishes respiratory rhythm bursting. Following 10 minutes of exposure to DAMGO, the "manipulation" period was initiated and the DAMGO exposure was continued at the same level as during the "baseline" period. After the "manipulation" period, the "recovery" period was initiated; DAMGO was removed from the superfusate at this point.

Potassium recordings collected throughout the experiments were converted from mV to mM as described in Section 2.2. Two main parameters were used to describe the experimental potassium dynamics: maximum concentration change and latency. The maximum concentration change describes the highest potassium concentration reached during the "manipulation" period, relative to the potassium concentration immediately prior to the initiation of the "manipulation" period. It is appropriate to consider a change relative to baseline, as opposed to the maximum potassium concentration reached, because the baseline concentration of potassium in the preBötC fluctuates between 3 and 5 mM (Richter

et al., 1978). The latency refers to the time necessary for this maximum concentration change to be realized after the initiation of the "manipulation" period.

5.3 Results

5.3.1 Dose-Response Relationship of DAMGO Application to Frequency

Application of DAMGO (1-250 nM) resulted in a dose-dependent decrease in normalized burst frequency (Figure 5.3), which is consistent with earlier findings (Gray *et al.*, 1999). In order to quantify this decrease of frequency as a function of dose, the mean normalized burst frequencies for each DAMGO concentration were plotted on a semi-logarithmic graph and fitted with a logarithmic function. Based on that function, the concentration of DAMGO that exhibited a 50% decrease in mean normalized burst frequency was 60 nM (Figure 5.4) with a Hill coefficient of 1.80.

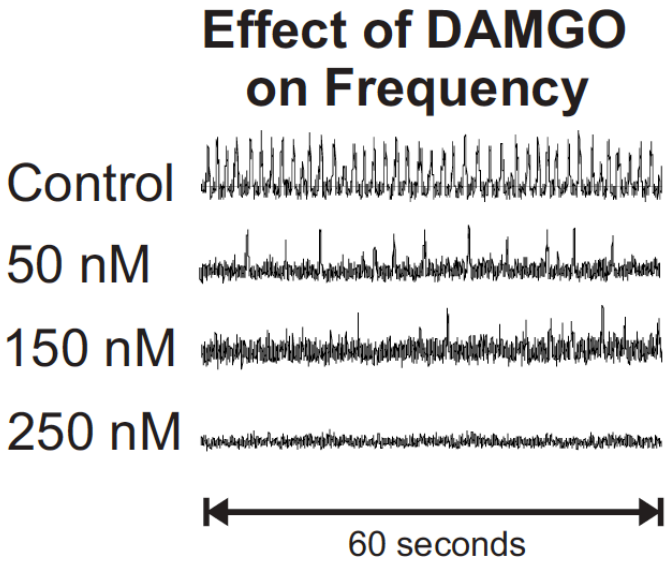

Figure 5.3 Application of the potent MOR agonist DAMGO to the preBötC resulted in a dose-dependent decrease in population burst frequency until complete cessation of bursting occurs (250 nM)

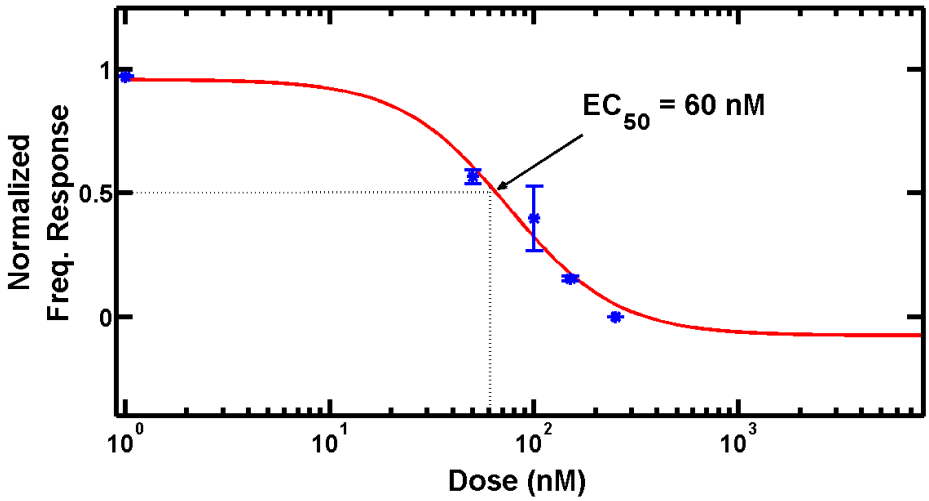

Figure 5.4 The dose-response curve relating decrease in the normalized burst frequency to DAMGO dose reveals the EC_{50} value for DAMGO is 60 nM with a Hill coefficient of 1.80.

5.3.2 Correlation of Extracellular Population Activity with Potassium Measurements

As previously mentioned, extracellular population (tonic) activity was recorded concurrently with potassium measurements (Figure 5.5).

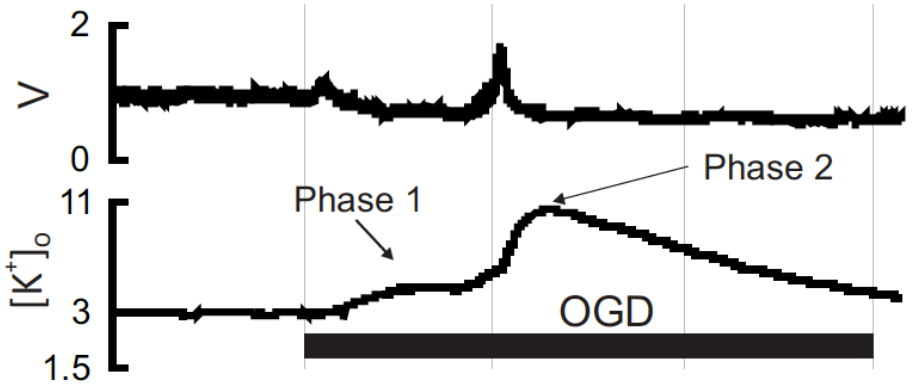

Figure 5.5 Increases in tonic activity (top trace) clearly correlated to increased extracellular potassium concentration (bottom trace). The biphasic extracellular potassium response to OGD, which has previously been described in literature, is clearly evident.

A biphasic accumulation of extracellular potassium during OGD has been previously described in literature (Hansen and Nedergaard, 1988). The potassium responses to OGD

presented in this chapter all followed this biphasic pattern. Phase 1 was initiated shortly after the onset of OGD and corresponded to a slight increase in extracellular population activity. Phase 2 correlated temporally to a large increase in extracellular population activity with the most rapid rise in extracellular potassium concentration occurring immediately subsequent to that increased activity.

5.3.3 Comparison in Potassium Accumulation Between Hypoxia and OGD

Biphasic increases in extracellular potassium concentration were observed both during hypoxia and OGD (Figure 5.6)

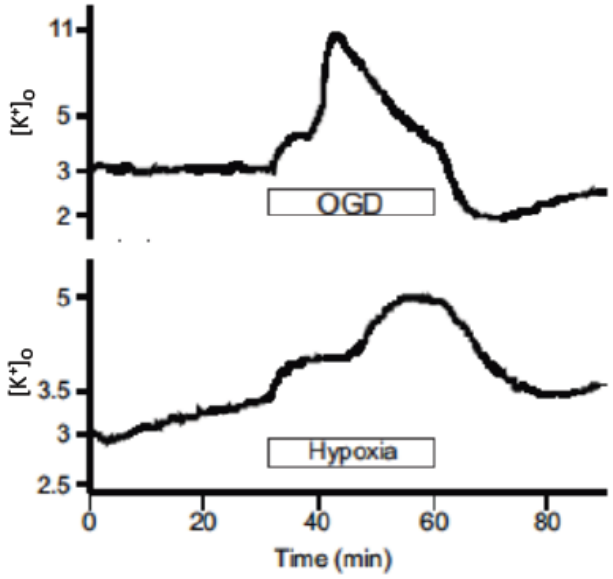

Figure 5.6 An increase in extracellular potassium concentration accompanied both hypoxia and OGD. However, the maximum change in extracellular concentration was greatly reduced in hypoxia, as compared to OGD. The time required to reach that maximum change in concentration was also increased significantly by hypoxia.

The maximum extracellular potassium concentration change was 4.18 +/ 0.44 mM (mean +/ S.D.) with a latency of 26.23 +/ 5.27 minutes for hypoxia, while the maximum extracellular potassium concentration change was 10.97 +/ 1.64 mM with a latency of 12.64 +/ 1.46

minutes for OGD. Therefore, both maximum concentration change and latency statistically differed between hypoxia and OGD ($p<0.05$).

5.3.4 Effect of DAMGO During OGD

In order to assess the effect of MOR activation during episodes of OGD, two concentrations of DAMGO were applied ten minutes prior to and during exposure to OGD. Both concentrations of DAMGO proved to have a statistically significant effect on maximum change in concentration and latency (Figures 5.7, 5.8).

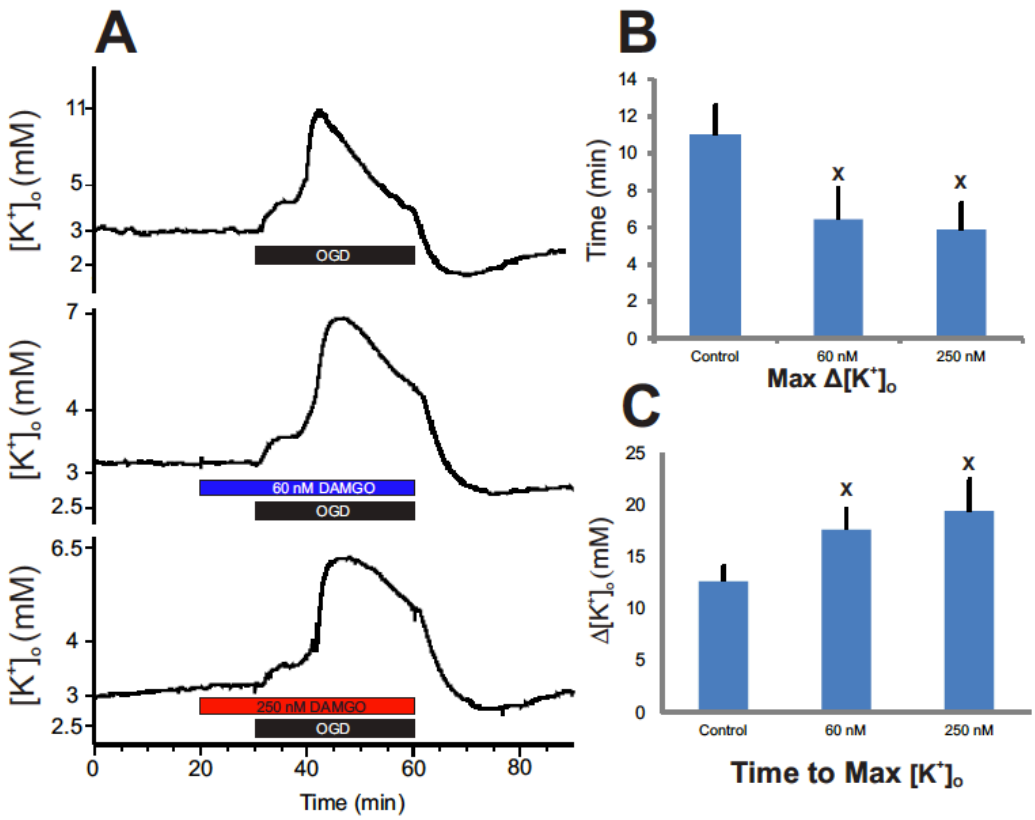

Figure 5.7 (A) The application of 60 nM DAMGO (middle trace) and 250 nM DAMGO (bottom trace) prior to and during episodes of OGD significantly modulated the accumulation of extracellular potassium compared with control (top trace). (B) There is a statistically significant difference (signified by 'X') in the maximum extracellular concentration reached during OGD between control trials and both concentrations of DAMGO. (C) There is a statistically significant difference (signified by 'X') in the time required to reach the maximum extracellular potassium concentration between control trials and both concentrations of DAMGO.

The maximum extracellular potassium concentration changes for 60 and 250 nM of DAMGO was 6.45 +/ 1.08 mM and 5.89 +/ 1.45 mM, respectively. The corresponding latencies were 17.65 +/ 1.99 minutes and 19.42 +/ 3.01 minutes, respectively. In control experiments, the maximum extracellular potassium concentration change was 10.97 +/ 1.63 mM with a latency of 12.64 +/ 1.46 minutes. Application of both concentrations of DAMGO produced a statistically significant change in maximum extracellular potassium concentration change and latency compared to control but there was no statistical significance between the DAMGO concentrations.

5.4 Discussion of Results

This research investigated the parameters of extracellular potassium accumulation in the pre-Bötzinger complex of the brainstem during periods of hypoxic and ischemic insult. The parameters used were the maximum extracellular potassium concentration reached during insult ($[K^+]_{max}$) and the time required to reach that potassium concentration following the onset of insult. To investigate whether these parameters were reasonable predictors of insult severity, they were assessed during periods of hypoxia and OGD. Compared to OGD, there was a significant decrease in $[K^+]_{max}$ and a significant increase in the time required to reach that concentration. These results may be due to the fact that glycolysis continues during hypoxia (but not OGD), thus inhibiting the release of glutamate (Kulik *et al.*, 2000).

It is well established that glutamate is a modulator or excitotoxicity-induced cellular death during episodes of OGD (Won *et al.*, 2002). The occurrence of OGD leads to a breakdown in sodium ion homeostasis (Rose *et al.*, 1998), which leads to an increase in

extracellular glutamate accumulation (Lipton and Rosenberg, 1994). Accordingly, sodium channel blockers have been shown to attenuate glutamate accumulation and neuronal death (Tsuchida *et al.*, 1996; Taylor *et al.*, 1995).

The research contained within this dissertation shows that MOR activation within the preBötC during periods of OGD significantly attenuates potassium ion homeostasis dysfunction. These results are similar to those previously published that show DOR activation in the cerebral cortex during OGD significantly modulates extracellular potassium accumulation (Chao *et al.*, 2007a; Chao *et al.*, 2007b; Chao and Xia, 2010). While Chao and colleagues suggest several possible mechanisms may contribute to the observed DOR-mediated neuroprotection, they showed conclusively that one of the mechanisms involved impaired sodium influx (Chao *et al.*, 2008) through a protein kinase C-dependent mechanism (Chao *et al.*, 2012).

While the mechanisms underlying MOR-mediated modulation of potassium homeostasis dysfunction are likely quite complex, it is interesting to note that MOR activation inhibits sodium currents by some of the same mechanisms as previously described by Chao and colleagues. And while Chao's group specifically concluded that MOR activation had no effect on neurons of the cortex during OGD (Chao *et al.*, 2007a), it is important to note that the cortex contain a higher density of DOR than other parts of the brain (Xia and Haddad, 1991). It is possible that this disproportionately high concentration of DOR may contribute to the neuroprotective effects of DOR activation during OGD in the cortex.

The correlation between opioid receptor density and neuroprotection has been previously investigated in the sea turtle. Compared to the mammalian brain, it is well

documented that the turtle brain displays remarkably diminished potassium homeostasis dysfunction when exposed to hypoxic stress (Xia *et al.*, 1992), thus conveying a tremendous capacity to resist anoxic damage (Jackson, 2000). The density of DOR in the cortex of the turtle is significantly higher than the cortex of the rat (Xia and Haddad, 2001), thus lending credence to the notion that the degree of DOR-mediated neuroprotection is directly dependent upon the DOR density. Having previously shown that MOR and DOR have similar effects on a variety of ion channels pertinent to ischemia-induced cellular death, it is reasonable to assume that MOR activation in an area of the brain with high MOR density has similar effects as DOR activation in the cerebral cortex during OGD.

The preBötC is a region of the brainstem that contains a high concentration of MOR (Gray *et al.*, 1999), and thus the conjecture that receptor density is implicated the neuroprotective effects of exogenous opioid application during OGD is indeed supported by the research in this chapter. While this research has shown that MOR activation in the preBötC during OGD significantly attenuates the accumulation of extracellular potassium, the mechanism of this protective action remains a mystery. It is indeed possible that MOR activation during OGD in the MOR-dense preBötC has a similar protective action as DOR activation during OGD in the DOR-dense cerebral cortex, as show by Chao and colleagues. However, for this link to become anything more than speculation, additional experimentation must be performed.

CHAPTER 6

OVERVIEW AND CONCLUDING REMARKS

The subject matter contained within this dissertation revolves around the flow of ions into and out of neural cells and the effect that flow has on the system. Specifically, this subject matter is investigated in the context of the following questions:

1. How does the flows of various ions and other charged particles affect the electrochemical characterization of the tissue by dielectric spectroscopy (DS) and how can this effect be accounted for?
2. Can the change in conductivity of the extracellular fluid as a function of neural insult severity provide insight into the health of the tissue?
3. Does pharmacological manipulation of the μ-opioid receptor attenuate the accumulation of extracellular potassium during oxygen glucose deprivation (OGD)?

Chapter by chapter, these questions were systemically investigated and answered.

The accumulation of extracellular ions accompanying diminished cellular health has drastic implications on the ability to characterize the tissue by DS. Not only does this accumulation affect the conductivity and dielectric permittivity of the tissue, it substantially contributes to the electrode polarization error. By implementing a novel superfusion system to constantly provide new, oxygenated extracellular solution, the health of the tissue is increased and the electrode polarization error is constant, thus increasing the ability to compare data from various trials.

As the health of neural cells diminish, their ability to maintain precise ionic gradients is diminished, which eventually leads to an accumulation of extracellular ions. The magnitude of this accumulation is directly proportional to the severity of the insult imparted upon the tissue. This extracellular ion accumulation is quantified by measuring the conductivity of the extracellular bathing fluid using dielectric spectroscopy.

The preBötC is a region of the brainstem that is responsible for respiratory rhythm genesis and sensitive to changes in oxygen and glucose concentration. When cells of the preBötC are deprived of oxygen and glucose, they respond by rapidly losing their ability to regulate potassium homeostasis. The resulting accumulation of extracellular potassium is directly related to the health of the tissue. Bath application of the potent MOR agonist DAMGO to the preBötC significantly attenuated the extracellular accumulation of potassium.

REFERENCES

Akhtari M, Salamon N, Duncan R, Fried I and Mathern G W 2006 Electrical Conductivities of the Freshly Excised Cerebral Cortex in Epilepsy Surgery Patients; Correlation with Pathology, Seizure Duration, and Diffusion Tensor Imaging *Brain Topography* **18** 281-90.

Alger B and Nicoll R 1981 A Simple Chamber for Recording from Submerged Brain Slices *Journal of Neuroscience Methods* **4** 153-6.

Ballanyi A V K and Richter D W 1995 Anoxic disturbance of the isolated respiratory network of neonatal rats *Experimental Brain Research* **103** 9-19.

Ballanyi K 2004 Protective role of neuronal K_{ATP} channels in brain hypoxia *The Journal of Experimental Biology* **207** 3201-12.

Berardelli A, Rothwell J, Day B and Marsden C 1985 Pathophysiology of Blepharospasm and Oromandibular Dystonia. *Brain* **108** 593-608.

Boom M, Niesters M, Sarton E, Aarts L, Smith T W and Dahan A 2012 Non-analgesic effects of opioids: opioid induced respiratory depression *Current Pharmaceutical Design* **18** 5994-6004.

Bordi F, Cametti C and Colby R H 2004 Dielectric spectroscopy and conductivity of polyelectrolye solutions *Journal of Physics: Condensed Matter* **16** R1423-R63.

Bordi F, Cametti C and Gili T 2001 Reduction of the contribution of electrode polarization effects in the radiowave dielectric measurements of highly conductive biological cell suspensions *Bioelectrochemistry* **54** 53-61.

Bortner C D, Hughes F M and Cidlowski J A 1997 A primary role for K^+ and Na^+ efflux in the activation of apoptosis *Journal of Biological Chemistry* **272** 32436-42.

Bot C and Prodan C 2009 Probing the membrane potential of living cells by dielectric spectroscopy *European Biophysics Journal* **38** 1049-59.

Brockmann H and Schmidt-Kastner G 1955 Valinomycin I, XXVII. Mitteil. über Antibiotica aus Actinomyceten *Chemische Berichte* **88** 57-61.

Caduff A, Dewarrat F, Talary M, Stalder G, Heinemann L and Feldman Y 2006 Non-invasive glucose monitoring in patients with diabetes: a novel system based on impedance spectroscopy *Biosensors and Bioelectronics* **22** 598-604.

Cametti C, Fratoddi I, Venditti I and Russo M V 2011 Dielectric relaxations of ionic thiol-coated noble metal nanoparticles in aqueous solutions: Electrical characterization of the interface *Langmuir* **27** 7084-90.

Chao D, Bazzy-Asaad A, Balboni G, Salvadori S and Xia Y 2008 Activation of DOR Attenuates Anoxic K^+ Derangement via Inhibition of Na^+ Entry in Mouse Cortex *Cerebral Cortex* **18** 2217-27.

Chao D, Bazzy-Asaad A, Balboni G and Xia Y 2007a δ-, but not μ-, opioid receptor stabilizes K^+ homeostasis by reducing Ca^{2+} influx in the cortex during acute hypoxia *Journal of Cellular Physiology* **212** 60-7.

Chao D, Donnelly D F, Feng Y, Bazzy-Asaad A and Xia Y 2007b Cortical δ-opioid receptors potentiate K^+ homeostasis during anoxia and oxygen–glucose deprivation *Journal of Cerebral Blood Flow & Metabolim* **27** 356-68.

Chao D, He X, Yang Y, Bazzy-Asaad A, Lazarus L H, Balboni G, Kim D H and Xia Y 2012 DOR activation inhibits anoxic/ischemic Na^+ influx through Na^+ channels via PKC mechanisms in the cortex *Experimental Neurology* **236** 228-39.

Chao D and Xia Y 2010 Ionic storm in hypoxic/ischemic stress: Can opiod receptors subside it? *Progress in Neurobiology* **90** 439-70.

Chen T and Hefter G 2003 Dielectric Spectroscopy of Aqueous Solutions of KCl and CsCl *Journal of Physical Chemistry A* **107** 4025-31.

Collingridge G L 1995 The brain slice preparation: a tribute to the pioneer Henry McIlwain. *Journal of Neuroscience Methods* **59** 5-9.

Coury L 1999 Conductance Measurements, Part 1: Theory *Current Separations* **18** 91-6.

Craig T J, Ashcroft F M and Proks P 2008 How ATP inhibits the open K(ATP) channel *Journal of General Physiology* **132** 131-44.

D'Mello S R, Galli C, Ciotti T and Calissano P 1993 Induction of apoptosis in cerebrallar granule neurons by low potassium: Inhibition of death by insulin-like growth factor I and cAMP *Proceedings of the National Academy of Sciences* **90** 10989-93.

D'Ambrosio R, Gordon D S and Winn H R 2001 Differential Role of KIR Channel and Na^+/K^+-Pump in the Regulation of Extracellular K^+ in Rat Hippocampus *Journal of Neurophysiology* **87** 87-102.

de Souza Wyse A T, Streck E l L, Worm P, Wajner A, Ritter F and Netto C A 2000 Preconditioning Prevents the Inhibition of Na^+,K^+-ATPase Activity after Brain Ischemia *Neurochemical Research* **25** 971-5.

Debye P and Hückel E 1923 Zur Theorie der Elektrolyte . I. Gefrieerpunktserniedrigung und verwandte Erscheinungen *Physikalische Zeitschrift* **24** 185-206.

Di Biasio A and Cametti C 2011 On the dielectric relaxation of biological cell suspensions: The effect of the membrane electrical conductivity *Colloids and Surfaces B: Biointerfaces* **84** 433-41.

Dobiszewski K F, Deek M P, Ghaly A, Prodan C and Hill A A 2012 Extracellular Fluid Conductivity Analysis by Dielectric Spectroscopy for In Vitro Determination of Cortical Tissue Vitality *Physiological Measurement* **33** 1249-60.

Dobiszewski K F, Shaker M R, Deek M P, Prodan C and Hill A A 2011 Design and implementation of a novel superfusion system for ex vivo characterization of neural tissue by dielectric spectroscopy (DS) *Physiological Measurement* **32** 195-207.

Du C, Yu M, Volkow N D, Koretsky A P, Fowler J S and Benveniste H 2006 Cocaine Increases the Intracellular Calcium Concentration in Brain Independently of Its Cerebrovascular Effects *The Journal of Neuroscience* **26** 11522-31.

Edvinsson L and Krause D N 2001 *Cerebral Blood Flow and Metabolism*: Lippincott Williams & Wilkins).

Egot-Lemaire S, Pijanka J, Sulé-Suso J and Semenov S 2009 Dielectric spectroscopy of normal and malignant human lung cells at ultra-high frequencies *Physics in Medicine and Biology* **54** 2341.

Foster K R and Schwan H P 1996 *Handbook of Biological Effects of Electromagnetic Fields,* ed C Polk and E Postow (Boca Raton, FL: CRC Press) pp 25-102.

Fröhlich F, Bazhenov M, Iragui-Madoz V and Sejnowski T J 2008 Potassium Dynamics in the Epileptic Cortex: New Insights on an Old Topic *The Neuroscientist* **14** 422-33.

Gabriel C 2007 *Bioengineering and Biophysical Aspects of Electromagnetic Fields* ed F S Barnes and G Ben (Boca Raton: CRC Press) pp 51-100.

Gabriel S, Lau R and Gabriel C 1996 The Dielectric Properties of Biological Tissues: II. Measurements in the Frequency Range of 10 Hz to 20 GHz *Physics in Medicine and Biology* **41** 2251-69.

Gennarelli T A 1986 Mechanisms and pathophysiology of cerebral concussion *The Journal of Head Trauma Rehabilitation* **1** 23-39.

Gersing E 1998 Impedance spectroscopy on living tissue for determination of the state of organs *Bioelectrochemistry and Bioenergetics* **45** 145-9.

Gheorghiu E 1993 The resting potential in relation to the equivalent complex permittivity of a spherical cell suspension *Physics in Medicine and Biology* **38** 979.

Gheorghiu E 1996 Measuring living cells using dielectric spectroscopy *Bioelectrochemistry and Bioenergetics* **40** 133-9.

Gheorghiu M and Gersing E 2002 Revealing alteration of membrane structures during ischema using impedance spectroscopy *Songklanakarin Journal of Science and Technology* **24** 777-84.

Goodman R R, Snyder S H, Kuhar M J and Young W S 1980 Differentiation of delta and mu opiate receptor localizations by light microscopic autoradiography *Proceedings of the National Academy of Sciences* **77** 6239-43.

Gray P A, Rekling J C, Bocchiaro C M and Feldman J L 1999 Modulation of Respiratory Frequency by Peptidergic Input to Rhythomgenic Neurons in the PreBötzinger Complex *Science* **286** 1566-8.

Haas H, Schaerer B and Vosmansky M 1979 A Simple Perfusion Chamber for the Study of Nervous Tissue Slices In Vitro *Journal of Neuroscience Methods* **1** 323-5.

Haddad G G and Donnelly D F 1990 O2 Deprivation Induces a Major Depolarization in Brain Stem Neurons in the Adult but not in the Neonatal Rat *Journal of Physiology* **429** 411-28.

Haddad G G and Yao H 2004 Calcium and pH homeostasis in neurons during hypoxia and ischemia *Cell Calcium* **36** 247-55.

Hajos N and Mody I 2009 Establishing a physiological environment for visualized in vitro brain slice recordings by increasing oxygen supply and modifying aCSF content *Journal of Neuroscience Methods* **183** 107-13.

Hansen A J 1985 Effect of Anoxia on Ion Distribution in the Brain *Physiological Reviews* **65** 101-48.

Hansen A J and Nedergaard M 1988 Brain Ion Homeostasis in Cerebral Ischemia *Neurochemical Pathology* **9** 195-202.

Hartley D M, Walsh D M, Ye C P, Diehl T, Vasquez S, Vassilev P M, Teplow D B and Selkoe D J 1999 Protofibrillar Intermediates of Amyloid beta -Protein Induce Acute Electrophysiological Changes and Progressive Neurotoxicity in Cortical Neurons *The Journal of Neuroscience* **19** 8876-84.

Heidlage J F and Jones A W 1981 The Kinetics of Ouabain-Sensitive Ionic Transport in the Rabbit Carotid Artery *Journal of Physiology* **317** 243-62.

Heinemann U and Lux H D 1977 Ceiling of stimulus-induced rises of extracellular potassium concentration in the cerebral cortex of cat *Brain Research* **120** 231-49.

Hertz L 2008 Bioenergetics of cerebral ischemia: a cellular perspective *Neuropharmacology* **55** 289-309.

Hibino H, Inanobe A, Furutani K, Murakami S, Findlay I and Kurachi Y 2010 Inwardly Rectifying Potassium Channels: Their Structure, Function, and Physiological Roles *Physiological Reviews* **90** 291-366.

Higashi K, Fujita A, Inanobe A, Tanemoto M, Doi K, Kubo T and Kurachi Y 2001 An inwardly rectifying K^+ channel, Kir4.1, expressed in astrocytes surrounds synapses and blood vessels in brain *American Journal of Physiology- Cell Physiology* **281** C922-C31.

Hitoshi S, Takeshi S, Ching-Chou W, Tomoyuki Y, Tomokazu M, Hiroyoski H, Masaki Y, Hiroyuki A and Hiroshi Y 2005 Oxygen Permeatbility For Poly(Dimethylsiloxane) (PDMS) Characterized by Feedback-Mode Scanning Electrochemical Microscopy *Chemical Sensors* **21** 49-51.

Hodgkin A L and Huxley A F 1952 Propagation of electrical signals along giant nerve fibres *Proceedings of the Royal Society of London* **140** 177-83.

Hodgkin A L and Keynes R D 1955 The Potassium Permeability of Giant Nerve Fibre *Journal of Physiology* **128** 61-88.

Husted R F and Reed D J 1977 Regulation of Cerebrospinal Fluid Bicarbonate By the Cat Choroid Plexus *Journal of Physiology* **267** 411-28.

Ikeda K, Kobayashi T, T. I, Usui H and Kumanishi T 1995 Functional Couplings of the δ- and the κ-Opioid Receptors with the G-Protein-Activated K+ Channel *Biochemical and Biophysical Research Communications* **208** 302-8.

Jackson D 2000 Living without oxygen: lessons from the freshwater turtle *Comparative Biochemistry and Physiology - Part A: Molecular & Integrative Physiology* **125** 299-315.

Jiang C, Agulian S and Haddad G G 1992 Cl^- and Na^+ homeostasis during anoxia in rat hypoglossal neurons: intracellular and extracellular in vitro studies *Journal of Physiology* **448** 697-708.

Jones H C and Keep R F 1987 The Control of Potassium Concnetration in the Cerebrospinal Fluid and Brain Interstitial Fluid of Developing Rats *Journal of Physiology* **383** 441-53.

Kaatze U and Feldman Y 2006 Broadband dielectric spectroscopy of liquids and biosystems *Measurement Science and Technology* **17** R17-R35.

Kang X, Chao D, Gu Q, Ding G, Wang Y, Balboni G, Lazarus L H and Xia Y 2009 δ-opioid receptors protect from anoxic disruption of Na^+ homeostasis via Na^+ channel regulation *Cell and Molecular Life Science* **66** 3505-16.

Kettenmann H, Sonnhof U and Schachner M 1983 Exclusive potassium dependence of the membrane potential in cultured mouse oligodendrocytes *The Journal of Neuroscience* **3** 500-5.

Kety S 1957 *Biochemistry of the Developing Nervous System,* ed D Richter (London, UK: Pergamon) pp 221-37.

Kochanek K D, Xu J, Murphy S L, Minino A M and Kung H-C 2012 Deaths: Final Data for 2009. ed U S D o H a H Services (Hyattsville, MD: Centers For Disease Control and Prevention).

Korff J M, Siebens A W and Gill J R J 1984 Correction of hypokalemia corrects the abnormalities in erythrocyte sodium transport in Bartter's syndrome *Journal of Clinical Investigations* **74** 1724-9.

Kromer W 1993 Mu opioid receptors modulate net chloride secretion in the guinea pig colonic mucosa in a dual fashion *Life Sciences* **53** 1061-8.

Kulik A, Trapp S and Ballanyi K 2000 Ischemia But Not Anoxia Evokes Vesicular and Ca^{2+}-Independent Glutamate Release In the Dorsal Vagal Complex In Vitro *Journal of Neurophysiology* **83** 2905-15.

Kuwabara S, Kanai K, Sung J-Y, Ogawara K, Hattori T, Burke D and Bostock H 2002 Anoxal hyperpolarization associated with acute hypokalemia: Multiple excitability measurements as indicators of the membrane potential of human axons *Muscle & Nerve* **26** 283-7.

Lee R M, Choi H, Shin J-S, Kim K and Yoo K-H 2009 Distinguishing between apoptosis and necrosis using a capacitance sensor *Biosensors and Bioelectronics* **24** 2586-91.

Lipton S and Rosenberg P 1994 Excitatory amino acids as a final common pathway for neurological disorders *New England Journal of Medicine* **330** 613-21.

Liu D, Slevin J R, Lu C, Chan S L, Hansson M, Elmer E and Mattson M P 2003 Involvement of mitochondrial K^+ release and cellular efflux in ischemic and apoptotic neuronal death *Journal of Neurochemistry* **86** 966-79.

Lorier A R, Huxtable A, Wilbur C, Housley G, Lipski J and Funk G 2007 Potent excitation of inspiratory frequency by P2Y1 receptor activation in the preBotzinger complex (PBC) *The FASEB Journal* **21** 918-30.

Magyar J P, Bartsch U, Wang Z-Q, Howells N, Aguzzi A, Wagner E F and Schachner M 1994 Degeneration of neural cells in the central nervous system of mice deficient in the gene for the adhesion molecule on glia, the β2 subunit of murine Na,K-ATPase *Journal of Cell Biology* **127** 835-45.

Markx G H and Davey C L 1999 The dielectric properties of biological cells at radiofrequencies: Applications in biotechnology *Enzyme and Microbial Technology* **25** 161-71.

Miyamoto O and Auer R N 2000 Hypoxia, hyperoxia, ischemia, and brain necrosis *Neurology* **54** 362-71.

Mohan M S and Bates R G 1975 Calibration of Ion-Selective Electrodes for Use in Biological Fluids *Clinical Chemistry* **21** 864-72.

Morawietz G, Kuwana K B S and Richter D W 1995 Oxygen supply and ion homeostasis of the respiratory network in the in vitro perfused brainstem of adult rats *Experimental Brain Research* **106** 265-74.

Morrison B M 2008 *Cerebrospinal fluid in clinical practice,* ed D N Irani (Philadelphia: Saunders Elsevier) p 12.

Müller M and Somjen G G 2000 Na^+ and K^+ Concentrations, Extra- and Intracellular Voltages, and the Effect of TTX in Hypoxic Rat Hippocampal Slices *Journal of Neurophysiology* **83** 735-45.

Murai Y, Ishibashi H, Koyama S and Akaike N 1997 Ca^{2+}-Activated K^+ Currents in Rat Locus Coeruleus Neurons Induced by Experimental Ischemia, Anoxia, and Hypoglycemia *Journal of Neurophysiology* **78** 2674-81.

Neusch C, Papadopoulos N, Müller M, Maletzki I, Winter S M, Hirrlinger J, Handschuh M, Bähr M, Richter D W, Kirchhoff F and Hülsmann S 2006 Lack of the Kir4.1 Channel Subunit Abolishes K^+ Buffering Properties of Astrocytes in the Ventral Respiratory Group: Impact on Extracellular K^+ Regulation *Journals of Neurophysiology* **95** 1843-52.

North R A, Williams J T, Surprenant A and Christie M J 1987 μ and δ receptors belong to a family of receptors that are coupled to potassium channels *Proceedings of the National Academy of Sciences* **84** 5487-91.

O'Rourke A P, Lazebnik M, Bertram J M, Converse M C, Hagness S C, Webster J G and Mahvi D M 2007 Dielectric properties of human normal, malignant and cirrhotic liver tissue: in vivo and ex vivo measurements from 0.5 to 20 GHz using a precision open-ended coaxial probe *Physics in Medicine and Biology* **52** 4707-19.

Pamenter M E and Buck L T 2008 delta-Opioid receptor antagonism induces NMDA receptor-dependent excitotoxicity in anoxic turtle cortex *Journal of Experimental Biology* **211** 3512-7.

Pamenter M E, Shin D S, Cooray M and Buck L T 2008 Mitochondrial ATP-sensitive K^+ channels regulate NMDAR activity in the cortex of the anoxic western painted turtle *Journal of Physiology* **586** 1043-58.

Penn J W and Bell E L 1978 Electrical Parameter Values of Some Human Tissues in the Radiofrequency Radiation Range. ed U S o A Medicine (Brooks Air Force Base: United States Air Force).

Prodan C and Bot C 2009 Correcting the Polarization Effect in Very Low Frequency Dielectric Spectroscopy *Journal of Physics D: Applied Phsyics* **42** 175505-15.

Prodan C, Mayo F, Claycomb J R, Miller J H and Benedik M J 2004 Low-frequency, low-field dielectric spectroscopy of living cell suspensions *Journal of Applied Physics* **95** 3754-6.

Purves D, Augustine G J, Fitzpatrick D, Hall W C, LaMantia A-S, McNamara J O and White L E 2008 *Neuroscience* (Sunderland, MA: Sinauer Associates, Inc.).

Ramirez J M, Quellmalz U J and Richter D W 1996 Postnatal changes in the mammalian respiratory network as revealed by the transverse brainstem slice of mice *Journal of Physiology* **491** 799-812.

Raynor K, Kong H, Chen Y, Yasuda K, Yu L, Bell G I and Reisine T 1994 Pharmacological characterization of the cloned kappa-, delta-, and mu-opioid receptors *Molecular Pharmacology* **45** 330-4.

Remillard C V and Yuan J X-J 2004 Activation of K^+ channels: an essential pathway in programmed cell death *American Journal of Physiology- Lung Cellular and Molecular Physiology* **286** L49-67.

Richerson G and Messer C 1995 Effect of Composition of Experimental Solutions on Neuronal Survival During Rat Brain Slicing *Experimental Neurology* **131** 133-43.

Richter D W, Camerer H and Sonnhof U 1978 Changes in extracellular potassium during the spontaneous activity of medullary respiratory neurons. *Pflügers Archiv European Journal of Physiology* **376** 139-49.

Ron A, Singh R R, Fishelson N, Shur I, Socher R, Benayahu D and Shacham-Diamand Y a 2008 Cell-based screening for membranal and cytoplasmatic markers using dielectric spectroscopy *Biophysical Chemistry* **135** 59-68.

Rose C R, Waxman S G and Ransom B, R. 1998 Effects of Glucose Deprivation, Chemical Hypoxia, and Simulated Ischemia on Na^+ Homeostasis in Rat Spinal Cord Astrocytes *The Journal of Neuroscience* **18** 3554-62.

Rossier B C, Geering K and Kraehenbuhl J P 1987 Regulation of the sodium pump: how and why? *Biochemical Sciences* **12** 483-7.

Ruangkittisakul A, Panaitescu B and Ballanyi K 2011 K^+ and Ca^{2+} dependence of inspiratory-related rhythm in novel calibrated mouse brainstem slices *Respiratory Physiology and Neurobiology* **175** 37-48.

Santhakumar V, Voipio J, Kaila K and Soltesz I 2003 Post-traumatic hyperexcitability is not caused by impaired buffering of extracellular potassium *Journal of Neuroscience* **23** 5865-76.

Schaefer M, Gross W, Ackemann J and Gebhard M 2002 The complex dielectric spectrum of heart tissue during ischemia *Bioelectrochemistry* **58** 171-80.

Schmid G, Neubauer G and Mazal P R 2003 Dielectric properties of human brain tissue measured less than 10 h postmortem at frequencies from 800 to 2450 MHz *Bioelectromagnetics* **24** 423-30.

Schwan H 1957 *Advances in Biological and Medical Physics,* ed J L Tobias (New York, NY: Academic Press) pp 147-209.

Sick T J, Rosenthal M, LaManna J C and Lutz P L 1982 Brain potassium ion homeostasis, anoxia, and metabolic inhibition in turtles and rats *American Journal of Physiology-Regulatory, Integrative and Comparative Physiology* **243** R281-R8.

Smith J C, Ellenberger H H, Ballanyi K, Richter D W and Feldman J L 1991 Pre-Bötzinger complex: a brainstem region that may generate respiratory rhythm in mammals *Science* **254** 726-9.

Solomon I C 2002 Modulation of gasp frequency by activation of pre-Bötzinger complex in vivo *Journal of Neurophysiology* **87** 1664-8.

Solomon I C, Edelman N H and Neubauer J A 2000 Pre-Bötzinger Complex Functions as a Central Hypoxia Chemosensor for Respiration In Vivo *The Journal of Neurophysiology* **83** 2854-68.

Somjen G G 2002 Ion Regulation in the Brain: Implications for Pathophysiology *Neuroscientist* **8** 254-67.

Su X, Wachtel R E and Gebhart G F 1998 Inhibition of calcium currents in rat colon sensory neurons by κ- but not μ- or δ-opioids *Journal of Neurophysiology* **80** 3112-9.

Takahashi H, Manaka S and Sano K 1981 Changes in extracellular potassium concentration in cortex and brain stem during the acute phase of experimental closed head injury *Journal of Neurosurgery* **55** 707-17.

Taylor C, Burke S and Weber M 1995 Hippocampal slices: glutamate overflow and cellular damage from ischemia are reduced by sodium channel blockade *Journal of Neuroscience Methods* **59** 121-8.

Teppema L J and Dahan A 2010 The Ventilatory Response to Hypoxia in Mammals: Mechanisms, Measurement, and Analysis *Physiological Reviews* **90** 675-754.

Thompson R J, Zhou N and MacVicar B A 2006 Ischemia Opens Neuronal Gap Junction Hemichannels *Science* **312** 924-7.

Toselli M, Toselli P and Taglietti V 1997 μ and δ opioid receptor activation inhibits ω-conotoxin-sensitive calcium channels in a voltage-and time-dependent mode in the human neuroblastoma cell line SH-SY5Y. *Pflügers Archiv European Journal of Physiology* **433** 587-96.

Tosteson D C, Cook P, Andreoli T and Tieffenberg M 1967 The Effect of Valinomycin on Potassium and Sodium Permeability of K and LK Sheep Red Cells *The Journal of General Physiology* **50** 2513-25.

Tryba A K, Pena F and Ramirez J-M 2003 Stabilization of Bursting in Respiratory Pacemaker Neurons *The Journal of Neuroscience* **23** 3538-46.

Tsuchida E, Harms J, Woodward J and Bullock R 1996 A use-dependent sodium channel antagonist, 619C89, in reduction of ischemic brain damage and glutamate release after acute subdural hematoma in the rat *Journal of Neurosurgery* **85** 104-11.

van Mil H, van Heukelomb J S and Bierc M 2003 A bistable membrane potential at low extracellular potassium concentration *Biophysical Chemistry* **106** 15-21..

Varghese A 2000 *The Biomedical Engineering Handbook: Second Edition,* ed J D Bronzino (Boca Raton: CRC Press).

Walz W 2000 Role of astrocytes in the clearance of excess extracellular potassium *Neurochemistry International* **36** 291-300.

Warny M and Kelly C P 1998 Monocytic cell necrosis is mediated by potassium depletion and caspase-like proteases *American Journal of Physiology- Cell Physiology* **276** C717-C24.

Wei L, Yu S P, Gottron F, Snider J, Zipfel G J and Choi D W 2003 Potassium Channel Blockers Attenuate Hypoxia- and Ischemia-Induced Neuronal Death *Stroke* **34** 1281-6.

White W, Nadler J and Cotman C 1978 A Perfusion Chamber for the study of CNS Physiology and Pharmacology in vitro. *Brain Research* **152** 591-6.

Witkowski G and Szulczyk P 2006 Opioid μ receptor activation inhibits sodium currents in prefrontal cortical neurons via a protein kinase A- and C-dependent mechanism *Brain Research* **1094** 92-106.

Won S J, Kim D Y and Gwag B J 2002 Cellular and Molecular Pathways of Ischemic Neuronal Death *Biochemistry and Molecular Biology* **35** 67-86.

Wong J R 2006 Lethal Injection Protocols: The Failure of Litigation to Stop Suffering and the Case for Legislative Reform *Temple Journal of Science, Technology & Environmental Law* **25** 263.

Xia Y and Haddad G G 1991 Ontogeny and distribution of opioid receptors in the rat brainstem *Brain Research* **549** 181-93.

Xia Y and Haddad G G 2001 Major difference in the expression of μ- and δ-opioid receptors between turtle and rat brain *Journal of Comparative Neurology* **436** 202-10.

Xia Y, Jiang C and Haddad G G 1992 Oxidative and glycolytic pathways in rat (newborn and adult) and turtle brain: role during anoxia *American Journal of Physiology-Regulatory, Integrative and Comparative Physiology* **262** R5950-R603.

Yamada K and Inagaki N 2005 Neuroprotection by KATP channels *Journal of Molecular and Cellular Cardiology* **38** 945-9.

Yamamoto C and McIlwain H 1966 Electrical Activities in Thin Sections from the Mammalian Brain Maintained in Chemically-Defined Media in vitro *Journal of Neurochemistry* **13** 1333-43.

Ye C, Walsh D M, Selkoe D J and Hartley D M 2004 Amyloid β-protein induced electrophysiological changes are dependent on aggregation state: N-methyl-D-

aspartate (NMDA) versus non-NMDA receptor/channel activation *Neuroscience Letters* **366** 320-5.

Young R S, During M J, Donnelly D F, Aquila W J, Perry V L and Haddad G G 1993 Effect of anoxia on excitatory amino acids in brain slices of rats and turtles: in vitro microdialysis *American Journal of Physiology- Regulatory, Integrative and Comparative Physiology* **264** R716-R9.

Yu S P, Yeh C-H, Strasser U, Tian M and Choi D W 1999 NMDA Receptor-Mediated K^+ Efflux and Neuronal Apoptosis *Science* **284** 336-9.

Zhang J, Gibney G T, Zhao P and Xia Y 2002 Neuroprotective role of δ-opioid receptors in cortical neurons *American Journal of Physiology- Cell Physiology* **282** C1225-C34.